Kaunas University of Technology

Faculty of Mechanical Engineering and Design

Research on Passenger Car Controlled Semi-Active Suspension and Business Analytics for an OEM Damper Manufacturing Industry

Master's Final Degree Project

Nalina Hamsaiyni Venkatesh

Project author

Dr. Andrius Dargužis

Supervisor

Kaunas, 2021

Kaunas University of Technology

Faculty of Mechanical Engineering and Design

Research on Passenger Car Controlled Semi-Active Suspension and Business Analytics for an OEM Damper Manufacturing Industry

Master's Final Degree Project

Vehicle Engineering (6211EX021)

Nalina Hamsaiyni Venkatesh

Project author

Dr. Andrius Dargužis

Supervisor

Prof. Dr. Artūras Keršys

Reviewer

Kaunas, 2021

Kaunas University of Technology

Faculty of Mechanical Engineering and Design

Nalina Hamsaiyni Venkatesh

Research on Passenger Car Controlled Semi-Active Suspension and Business Analytics for an OEM Damper Manufacturing Industry

Declaration of Academic Integrity

I confirm the following:

1. I have prepared the final degree project independently and honestly without any violations of the copyrights or other rights of others, following the provisions of the Law on Copyrights and Related Rights of the Republic of Lithuania, the Regulations on the Management and Transfer of Intellectual Property of Kaunas University of Technology (hereinafter – University) and the ethical requirements stipulated by the Code of Academic Ethics of the University;

2. All the data and research results provided in the final degree project are correct and obtained legally; none of the parts of this project are plagiarised from any printed or electronic sources; all the quotations and references provided in the text of the final degree project are indicated in the list of references;

3. I have not paid anyone any monetary funds for the final degree project or the parts thereof unless required by the law;

4. I understand that in the case of any discovery of the fact of dishonesty or violation of any rights of others, the academic penalties will be imposed on me under the procedure applied at the University; I will be expelled from the University and my final degree project can be submitted to the Office of the Ombudsperson for Academic Ethics and Procedures in the examination of a possible violation of academic ethics.

Nalina Hamsaiyni Venkatesh

Confirmed electronically

Kaunas University of Technology

Faculty of Mechanical Engineering and Design

Study programme: Vehicle Engineering (6211EX021)

Task Assignment of Master's Final Degree Project

Given to the student: Nalina Hamsaiyni Venkatesh

1. Title of the Project:

Research on Passenger Car Controlled Semi-Active Suspension and Business Analytics for an OEM Damper Manufacturing Industry

Lengvųjų automobilių valdomos pusiau aktyvios pakabos tyrimas ir verslo analizė OEM amortizatorių gamybos pramonėje

2. Aim of the Project: The research aims to design and analyze experimentally and analytically to validate an effective semi-active suspension system to isolate vibrations using magnetorheological fluid. To create a facility layout design for the proposed OEM damper, a small scale manufacturing industry to plan the functioning. To conduct business analytics to determine the market trend to evaluate the business flow.

3. Tasks of the Project: To propose an altered composition of the MR fluid to increase the damping performance. To experimentally prepare the nanomaterial and the nanofluid. To validate characters of the particles and fluid with suitable experimental tests. To fabricate a protype of MR fluid damper setup. To determine the damping performance of the proposed composition of MRF damper experimentally and analytically. To create a facility layout plan to estimate costs and plan functioning of the small scale industry. To perform business analytics tools to evaluate the sustainability of the product during launch and post launch period.

4. Structure of the Text Part:

Introduction
I. Literature Review
II. Magnetorhelogical Fluid Damper
III. Business Analytics
IV. Discussion, Challenges and Future Scope
Conclusion

References
Appendix

5. Consultants of the Project:

Author of the Final Degree Project	Nalina Hamsaiyni Venkatesh 2020-02-04 *(Name, Surname, Date)*
Supervisor of the Final Degree Project	Dr. Andrius Dargužis 2020-02-04 *(abbreviation of the position, name, surname, date)*
Head of Study Programme	Prof. Dr. Artūras Keršys 2020-02-04 *(abbreviation of the position, name, surname, date)*

Venkatesh, Nalina Hamsaiyni. Research on Passenger Car Controlled Semi-Active Suspension and Business Analytics for an OEM Damper Manufacturing Industry. Master's Final Degree Project / Supervisor Dr. Andrius Dargužis; Faculty of Mechanical Engineering and Design, Kaunas University of Technology.

Study field and area (study field group): Transport Engineering (E12), Engineering Science.

Keywords: Magnetorheological Suspension, Quarter Car Model Testing, MATLAB Simulink, Facility Layout Plan, Break-Even Analysis, Bass Diffusion Model.

Kaunas, 2021. Number of pages: 89

Summary

Recent advancements in the field of transport industry correspond to the research and development of mobility subsystems. In the suspension subsystem, the recent development and research is revolving around the active and semi-active suspension systems. Electrorheological and magnetorheological and electric and magnetic suspensions are in constant research for development. A complete literature review was carried out to determine the current research areas and scope in this field of transport development to serve the market needs. Conventional magnetorheological fluid damper (MR Fluid damper/ MRF damper) has some disadvantages such as fluid particle separation, oxidation of particles, clumping effect, hard cake formation, and behavioral stability of the fluid. In this research, an altered composition of the MR fluid to overcome the challenges faced with the conventional magnetorheological suspensions. The nano particles of nickel-iron oxide were prepared in the laboratory and based on the composition proposed the nano fluid was prepared. Synthesized nano particles were analyzed by scanning electron microscope. Rheological properties of the fluid were assessed by rheometer testing. The performance of the MR fluid in the damper setup was experimentally evaluated by quarter-car model setup and LABVIEW Signal Express software to dynamically stimulate the damper with virtual road vibrations to determine its capacity while being employed in transport. Vibrational damping efficiency of each sample for different input voltages and frequency of vibrations were determined to evaluate the optimum conditions. Market potential of the new MR fluid damper as a commercial product was analyzed by business analytical tools. The product is considered an OEM damper and the further business analytics part is carried out considering a small-scale OEM damper manufacturing industry to serve the transport industry to enhance the mobility features of a vehicle. A facility layout plan for the manufacturing industry was designed, based on which functioning and cost of the functioning were estimated. Based on the evaluated conditions, the breakeven quantity and year were determined. Prediction of sales and market growth of the sales was performed by implementing the Bass diffusion model of business. The predicted inclination period of the sales and the declension period of the sales are predicted using the Bass diffusion model for business.

Venkatesh, Nalina Hamsaiyni . Lengvųjų automobilių valdomos pusiau aktyvios pakabos tyrimas ir verslo analizė OEM amortizatorių gamybos pramonėje. Magistro baigiamasis projektas / Vadovas Dr. Andrius Dargužis, Mechanikos inžinerijos ir dizaino fakultetas. Kauno technologijos universitetas.

Studijų kryptis ir sritis (studijų krypčių grupė): Transporto inžinerija (E12), Inžinerijos mokslai.

Reikšminiai žodžiai: Magnetoreologinė pakaba, ketvirčio automobilio modelio testavimas, MATLAB „Simulink“, įrenginio išdėstymo planas, lūžio analizė, boso difuzijos modelis.

Kaunas, 2021. Puslapių sk. p. 89

Santrauka

Pažanga transporto sektoriaus vystymesi yra tiesiogiai susijusi su tyrimais ir eksperimentine plėtra, vykdomais atskiroms transporto rūšims. Kalbant apie automobilių pakabos sistemas, šiais laikais atliekama daug eksperimentinių tyrimų, nukreiptų į aktyvios ir pusiau aktyvios pakabos konstrukcijų tobulinimą. Būtent elektroreologinės ir magnetoreologinės bei elektrinės ir magnetinės pakabos yra šiuolaikinių tyrimų objektai. Tai patvirtina atlikta išsami literatūros apžvalga, leidusi suprasti naujausių tyrimų kryptis ir apimtis šių detalių gamybos sferoje, siekiačioje patenkinti rinkos poreikius. Įprastinį magnetoreologinį skystį naudojantys slopintuvai (MR slopintuvas / MRS slopintuvas) turi keletą trūkumų, tokių kaip skysčio dalelių separacija, dalelių oksidacija, kietų nuosėdų formavimasis ir skysčio elgsenos pokyčiai. Atliekant šį tyrimą, buvo pakeista MR skysčio sudėtis, taip siekiant įveikti iššūkius, su kuriais susiduria įprastos magnetoreologiniai slopintuvai. Nikelio-geležies oksido nano dalelės buvo paruoštos universiteto laboratorijoje. Jų pagrindu, pagal šiame darbe pasiūlytą sudėtį, buvo paruoštas nano skystis. Gautos nano dalelės buvo nuodugniai ištirtos elektroniniu mikroskopu, o reologinių skysčio savybių įvertinimui naudotas laboratorinis reometras. MR skysčio elgsenos įtaka slopintuvo veikimui eksperimentiškai įvertinta naudojant „Automobilio pakabos ketvirčio modelį” ir „LABVIEW Signal Express“ programinį paketą, kurių pagalba siekta imituoti dinaminį slopintuvo atsaką į virtualias nelygaus kelio paviršiaus keliamas vibracijas, taip parenkant ir užtikrinant reikiamus gaminio parametrus. Siekiant parinkti optimalias darbo sąlygas, buvo nustatytas kiekvieno mėginio vibracijos slopinimo efektyvumas skirtingoms įėjimo įtampoms ir vibracijų dažniui. Naujai sukurto MR skystį naudojančio slopintuvo rinkos potencialui įvertinti pasitelkti verslo analizės metodai. Priimta, kad rinkos dalyvis yra mažų įmonių kategorijai priskiriamas OEM gamintojas, gaminantis inovatyvius slopintuvus automobiliams, kurie gali pagerinti automobilio pakabos charakteristikas. Šiame darbe sukurtas gamybos įrenginių išdėstymo planas, pagal kurį optimizuotas linijos veikimas ir apskaičiuoti gamybos kaštai. Pagal šiuos kriterijus nustatytos sąsajos tarp įmonės sąnaudų, apimties ir pelno, įskaitant įmonės „Lūžio tašką“ (Breakeven quantity) ir „Lūžio metus“. Pardavimų ir rinkos augimo prognozavimas atliktas pasitelkus „Bass“ verslo difuzijos modelį. Šio modelio pagalba įvertinti prognozuojami pardavimų augimo bei mažėjimo periodai.

Table of Contents

List of Figures

List of Table

Introduction

Suspensions are the collective term assigned to the system consisting of the arrangement of the tires along with the linkages, springs, shock absorbers, or dampers that connect the vehicle frame to tires. The suspension system integrates the relative motion that deals with the uniformity of the ride experience between the car's frame and the wheels together. The suspension system provides vehicle handling parameters to a vehicle while cornering, maneuvering, and braking[1].

With the evolution and technological advancements, suspension system has evolved from a simple linkage to an advanced complex technologically adjusTable. damping suspension which provides intelligent damping to the vehicle according to the ride conditions. The simplest vehicle suspension consists of a rigid axle acting as a suspension to lift the frame when the vehicle experiences a bump. The complex advanced suspensions are capable of adjusted manually and automatically concerning the road and riding conditions[1].

A balanced suspension is engineered and mounted to absorb ground movements as shocks to have the required damping effect to achieve ride comfort and handling. The absorbed shocks affect the velocity and stability of the vehicle while in motion when not absorbed. To serve the purpose of delivering stability to a vehicle suspensions are mounted in a wheel assembly [2].

Suspension's came into exisitence with invention of high-speed internal combustion (IC) engines. The speed range of IC engines demanding a stability provider and a load carrier. When the technology advanced to produce a range of vehicles for a specific purpose, a suspension design had to adapt to the requirement. Thus different types of suspensions and their assemblies were designed, manufactured, and mounted to serve the expected performance of each vehicle type [1].

The suspension assembly as a system provides so much to the vehicle that now it is merely impossible to build a vehicle without a suspension system. Apart from offering and maintaining the ride handling, stability, safety, and performance, the suspension is the holding gauge of the whole sprung weight of the vehicle by giving balanced distribution on the wheels to hold against the gravity [6].

Industrial advancements and technological advancements involved in the process of suspensions have greatly increased. The demand in ride comfort parameters rule the vehicle sales, every vehicle design competes itself with the newer ones to undergo up-gradation. Though providing stability, safety, and performance during cornering, maneuvering, and braking is a vital role held by suspensions, the market needs are different. With every new vehicle, design evolves an altered or upgraded suspension system to deliver the expectations of customers to capture the market. The invested effort in the development department in every industry understands the importance of an integrated vehicle with a convincingly advanced technological suspension installed to them [7].

The compliance in suspension parameters along with the steering parameters and tire parameters contribute to the ride quality, stability, safety, and performance of a vehicle in terms of comfort and travel. The parameters namely roll center, camber angle, kingpin inclination, caster angle is critical while designing a suspension that will effectively integrate the function intended. The parameters are so designed that they provide compliance in integrating the subsystems of the vehicle. A vehicle must have

synchronized steering system and suspension to provide stability and control. The two systems together provide the vital characteristics - stability and ride comfort [9].

Aim of the research

To design and analyze an effective semi-active suspension system to isolate vibrations using magnetorheological fluid. To create a simple facility layout design for the proposed OEM damper, small scale manufacturing industry to plan the functioning and to conduct business analytics to analyze product sustainability in the market.

Tasks to reach aim of the research

1. To propose an altered composition of the MR fluid to increase the damping performance.
2. To experimentally prepare the nanomaterial and the nanofluid. To validate characters of the particles and fluid with suitable experimental tests.
3. To fabricate a protype of MR fluid damper setup.
4. To determine the damping performance of the proposed composition of MRF damper experimentally and analytically.
5. To create a facility layout plan to estimate costs and plan functioning of the small scale industry.
6. To perform business analytics tools to evaluate the sustainability of the product during launch and post launch period.

Novelty of the research

The novelty of the research lies in the composition of the MR fluid used for the damper; the particle characteristics are chosen to enhance the damping characteristics in comparison to the conventional MRF damper by eliminating oxidation and clumping of particles in the fluid and increasing the stability of the fluid.

1. Literature review

Aizuddin Fahmi Mohd Riduan et al. (2018) reviewed the different types of suspension systems available in commercial vehicles in their research. The review denotes that depending on the parametric quality achieved by the system arrangement was classified into different types namely: passive, semi-Active, and active. The overview includes the research in various new advancements in technology applied to the suspension system. The latest trends MR fluid dampers, hydraulic roll control, and active curve tilt Suspension was discussed. In this research, it is clearly stated that the semi-active suspension – MR Fluid dampers provides a high balance between ride quality performance and stability. The continuously varying damping adaptability concerning the road conditions is noted as a noble character [4].

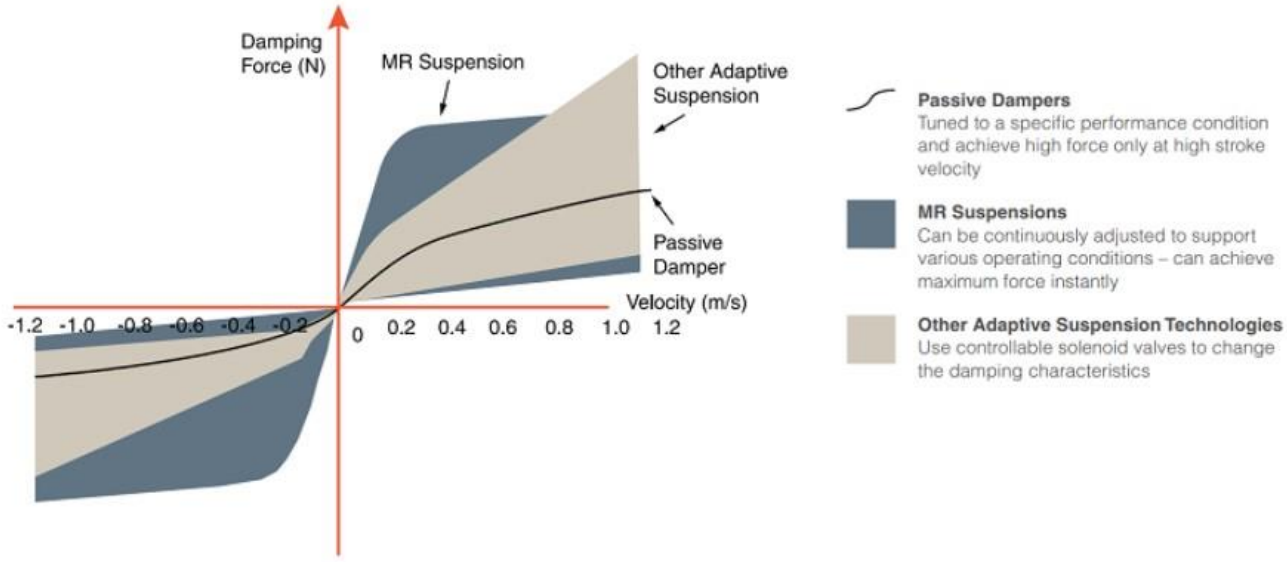

FIG. 1. Graphical damping performance comparison[4].

Pawel Skalski et al. (2017) investigated the magnetorheological dampers. The smart fluids that respond to changing magnetic or electric fields were employed in suitable applications of which the suspensions were one. The materials that have varying rheological properties with changes in the magnetic flux are the magnetorheological fluids. The MR fluid dampers and MR elastomer dampers are compared to determine their characteristics differences, advantages, and disadvantages. The MR Elastomers are polymer-based MR substances that remain in a solid state, unlike the MR fluid. According to this research, MR elastomers have the advantage over MR fluid as they are no threat to leakage, sealing is not a concern, material deposition, environmental concerns. Slowly MR fluids are substituted with MR elastomers. They concluded that, with research in new smart material composition to avoid the disadvantages of MR fluid, they can be used in many applications. Fig. 2 shows the Construction of the MR elastomer damper, where 1- Cylinder, 2- Piston Rod, 3-Piston, 4-Spacer Sleeve, 5-Shim, 6-MR Elastomer, 7- Lead, 8-Nut, 9-Marking Stick, 10-Nut, 11-Shim, 12-Clamp, 13-Rivet, 14-Nut, 15-Screw, 16-Magnet [8].

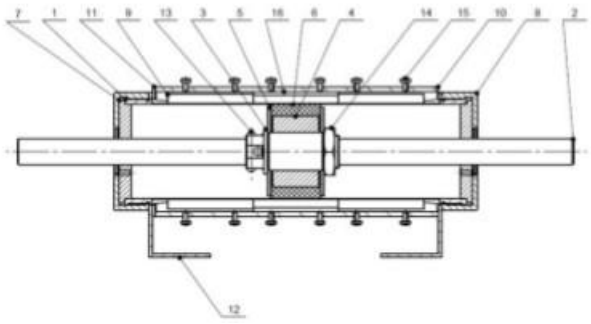

FIG. 2. Construction of MR elastomer damper [8]

Abhijeet N. Kulkarni Et al. (2013) investigated the fluid behavior of magnetorheological and electrorheological fluid using Ansys and CFD models for different action modes as conditions. The designed test model was a parallel plate and a parallel disc between which the fluid behavior was examined. The different test models adapted to examine the fluid behavior were the Bingham plastic model, Herchel-Bulkley model. The direct flow mode, shear mode and squeeze mode were used as the action modes in Fig. 3. The Newtonian and Non-Newtonian fluids were examined under the same conditions under the different action modes to conclude that the damping force and damper displacement for a Newtonian fluid were linear and for a Non-Newtonian fluid it was non-linear[9].

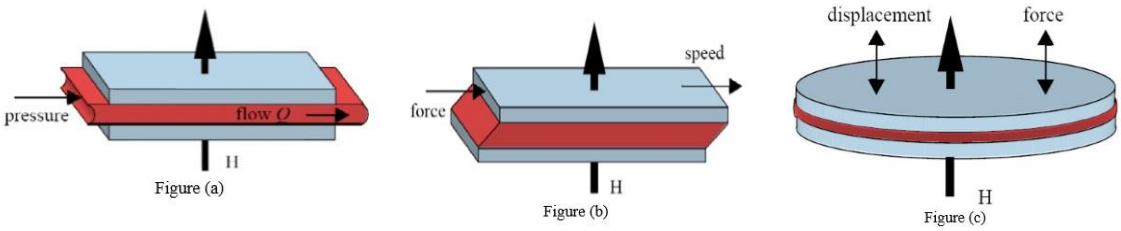

FIG. 3. (A) Direct flow mode (B) Shear mode (C) Squeeze mode [9]

Nikhil Desai et al. (2016) discussed the modeling and control strategies to determine the performance of a suspension system design. The experimental and analytical method of evaluating the performance of a suspension system was discussed. The experimental setup of a quarter car, half-car model, full car model suspension was exploited to determine the ability of the designed suspension system which was verified using an analytical method. Analytical verification was obtained using the MATLAB Simulink platform[10].

SA Wahid et al. (2016) investigated the defects and failures of the magnetorheological fluid. The enlisted defects are formation of hard cake, clumping effect, fluid particle separation, oxidation of particles, and stability. The mentioned disadvantages form the major area of focus as any change in the MR fluid composition should resolve at least one of the disadvantages to become more suitable for common usage [11]. To make any advancement in the MR Fluid damper it is mandatory to understand the characteristics and defects to focus on the effective outcome. Thus, a detailed explanation of the review of MR Fluid in Dampers is discussed below.

Hard Cake Formation is the phenomenon in which the magnetic particles in the fluid form a hard rigid solid cake state. This hard cake formation is due to the residual magnetic field in the particles even when

there is no magnetic field applied to the fluid. To overcome this, previous researchers have suggested using surfactants which reduced the hard cake formation. Recent research has denoted that the mixture of nanoparticles with a combination of microparticles can greatly influence the hard cake formation[11].

During the squeeze mode analysis, it was determined that the magnetic particles form clumps or clusters on repeated cycles of magnetic field response in a rheometer testing to determine the rheological properties of the fluid. It was evident that the density of the magnetic particles in a particular area was increased as they formed clumps. Fig. 4 shows the clumping in the MR Fluid under repeated cycles of tests[11].

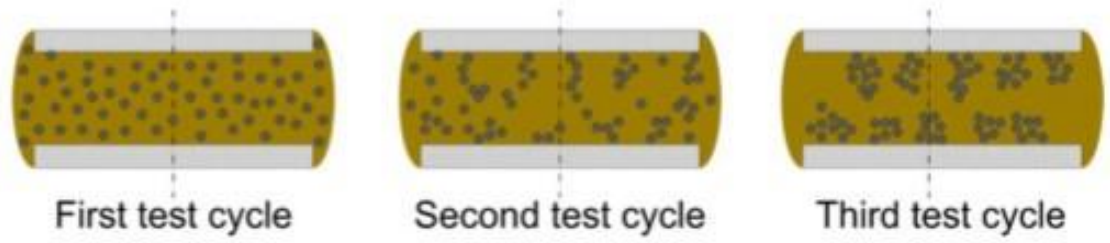

FIG. 4. Clumping effect [11]

The impulsive behavior of the fluid when subjected to compressive force on squeeze mode where the stress-strain relationship of the same composition liquid varied with a change in intensity of the magnetic flux strength. This behavior is termed Fluid Particle Separation. This phenomenon is linked to the clumping effect, as the density of the magnetic particle in a given particular area differs with cycle, the behavior related to their structure and orientation also varies which gives rise to the Fluid Particle Separation. Fig. 5 shows the variation in the stress-strain curves [11].

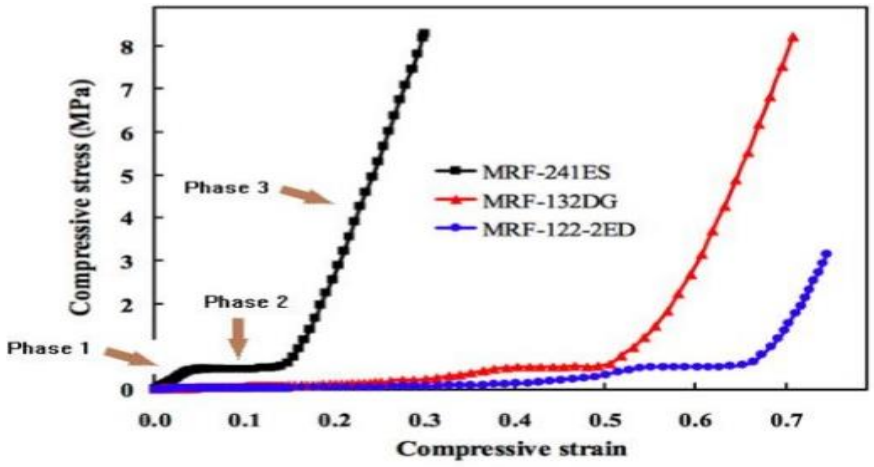

FIG. 5. Fluid particle separation [11]

Oxidation Particles are the characteristic of any iron material. The MR Fluid contains about 20-40% Magnetic particles of which mostly iron and iron oxides are employed to obtain the best response behavior. The iron particles suspended in the carrier fluid are isolated from the environment, but when there are high-temperature changes or in the case of atmospheric exposure these particles are prone to

undergo oxidation due to the availability of oxygen. SA Wahid et al., researched to estimate the quantity of oxygen and oxidation reaction time [11].

They have enumerated the difference in stability obtained at different temperatures, different surfactants, and time. The different use of nonmagnetic additives and magnetic additives with different sizes greatly influenced the stability of the fluid. Being a non-Newtonian fluid, stability is nonlinear[11].

In G.Z. Yao et al. (2002) in their experimental and analytical research, have used the Bouc-Wen Model as a mathematical model and the quarter car model as the experimental setup to determine the damping coefficient, damping force, displacement obtained for various applied current. With the obtained parameters relationships were established to study the ability of the analyzed MR Fluid Damper. The mathematical model Bouc-Wen was employed in the MATLAB Simulink model to determine the frequency, damping force, displacement analytically. The experimental and analytical results were examined to determine whether the system abides by the Bouc-Wen Mathematical Model. Fig.s 6 and 7 show the Bouc-Wen Model and Quarter Car Model. From these experiments, to conclude the acceleration response of sprung mass, suspension travel, tire deflection is effectively controlled around the body resonance[12].

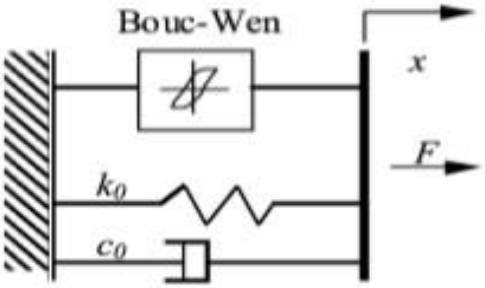

Fig. 6. Bouc-Wen model [12]

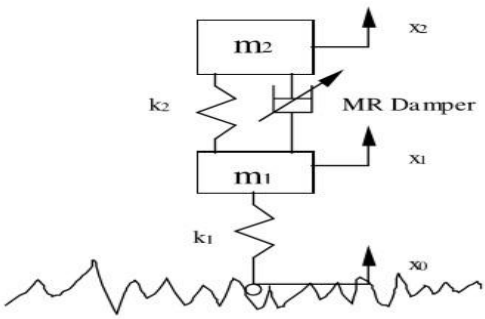

FIG. 7. Quarter car model [12]

Zohir BenLahcene et al. (2008) performed different semi-active suspension system control policies such as a skyhook, ground-hook, and hybrid on half vehicle models with 2-axle, 3-axle, 4-axle to determine the different ride comfort, suspension travel, road-handling in time and frequency domains. In comparison to the skyhook and ground-hook, the hybrid model yields better comfort and ride handling performance concerning suspension travel. The skyhook improves both sprung and unsprung mass

responses. Ground-hook state takes a long time to settle. Thus, to conclude the higher the number of axles shows a distinct improvement in the characteristic responses in some models[13].

According to Mohammad Meftahul Ferdaus et al (2015) their research and investigation through experimentation to determine the force delivered by the MRF damper at different viscosities. The viscosity of the MRF is varied which resulted in a proportional change to the applied magnetic flux or excitation current. The force delivered varied at different stroke lengths and in different stroke rates. The experimental setup consisted of the UTM – Universal Testing Machine with a current control circuit to vary the viscosity and TRAPEZIUMX software was used to obtain the signal output. The load sensor in UTM was used to obtain the displacement values. This setup is as shown in Fig. 8[14].

FIG. 8. UTM setup [14]

Sidharth Sharma et al. (2017) examined the properties of the MR Damper and their potential applications. As semi-active suspension performs better than passive and active suspension types, these are preferred in vehicles to enhance the ride quality, handling and performance. Based on the specific utilization the apt MRF damper is used to obtain utmost performance. It is very reliable and can be used in structural applications such as in bridges to arrest vibrations providing isolated sprung systems in Fig. 9[15].

FIG. 9. Donting lake bridge – China [15]

MR Fluids can be applied to armor Vests to protect oneself from attacks. The vest is light and easy until the magnetic is applied. When the magnetic strength is applied it hardens in milliseconds to produce lifesaving armor as shown in Fig. 10. MR Fluids are also employed in Prosthetic limbs as they are highly responsive in lesser time when compared to the conventional stepper motor in Fig. 11 making stairs and slopes easier for prosthetic limb users [15].

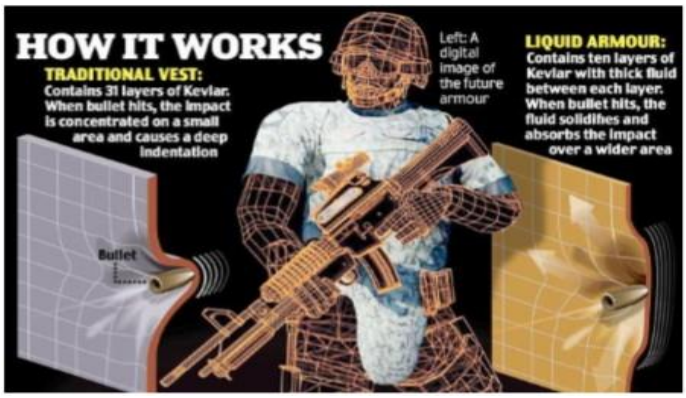

FIG. 10. MR fluid armour vest [15]

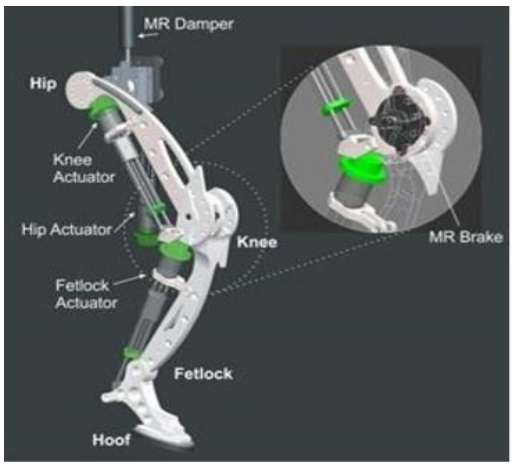

FIG. 11. Prosthetic limbs [15]

In Bogdań Sapiński et al. (2013) their experiment to determine the dependency of the height of the gap in the Squeeze mode in a CFD model. Squeeze mode testing was conducted where one plate was stationary whilst the other moved in a progressive retractive motion. This test was derived from the Bingham model, which does not account for the change in yield stress due to the change in height of the gap in Fig. 12[16].

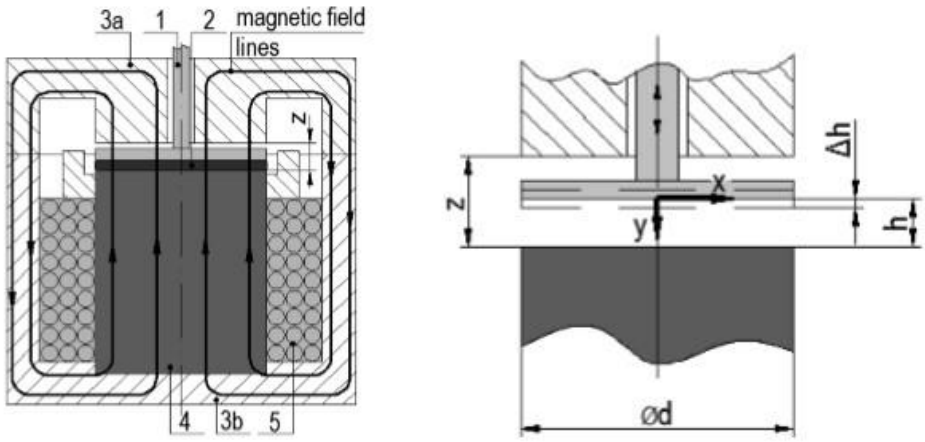

FIG. 12. Squeeze model using Bingham model [16]

Sadak Ali Khan et al. (2014) have also discussed the design of semi-active suspension control based on Annular Duct, Herschel-Bulkley model, Bingham Model for the flow mode, shear mode, squeeze mode, and combined flow and shear mode. To avoid bearing malfunction, temperature rise, current fluctuation, short-circuiting it is inevitable. to insulate. To overcome these two end collars can be employed[17].

G.R. Peng et al. (2014) conducted a study to examine the force lag phenomenon on the MRF Damper using the Bouc-Wen Mathematical Model to determine a basic hysteretic loop to compare with the proposed Bouc-Wen-Baber-Noori Model to overcome the disadvantage to determine the accurate force-lag relationship[18].

X.C. Guan et al. (2011) model and analyzed the method to predict the damping force-velocity hysteresis curve of MR dampers. This study was done under sinusoidal displacement excitation. This formulation of the determination of hysteresis width neglected the viscosity. It was found and concluded that the hysteresis width was dependent on the spring stiffness alone for sinusoidal displacement and was not affected by the area of the piston. The determined design of the hysteresis in Fig. 13[19].

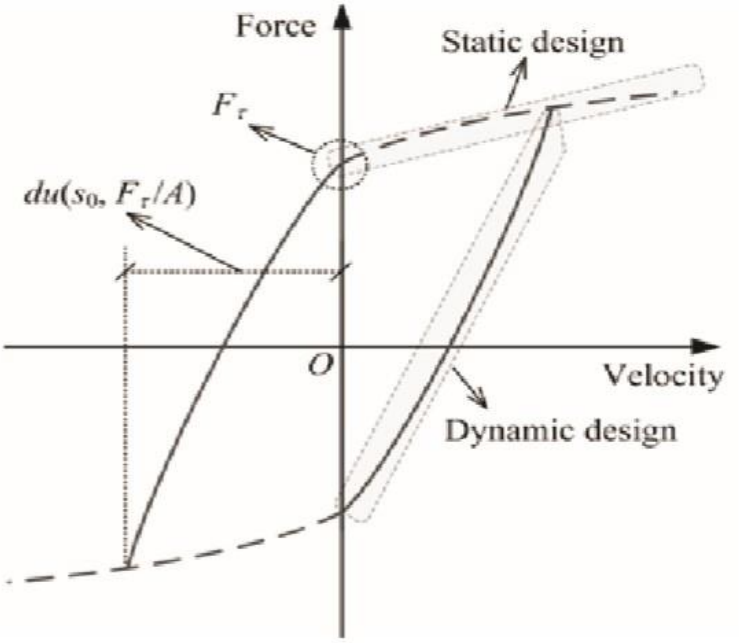

FIG. 13. Hysteresis of a MR fluid damper [19]

T.Imthiyaz Ahamed et al. (2014) in their innovative application of MR dampers, have proved the capabilities of reliability and stability. The MRF damper were employed in bumpers as an impact absorbing component to isolate the vibration and impact caused during a collision. The design factors and parameters and control model for the varying magnetic field intensity depending on the rate of collision are designed according to the requirements. The performance of the MRF as an impact resistor is assessed and evaluated[20].

R.N.Yerrawar et al. (2014) conducted a study on the MR Damper using the Bingham Model in Fig. 14. The model was simulated and the obtained resulted in a lower sprung mass acceleration for road excitations. This model was concluded to provide good passenger comfort and vehicle stability[21].

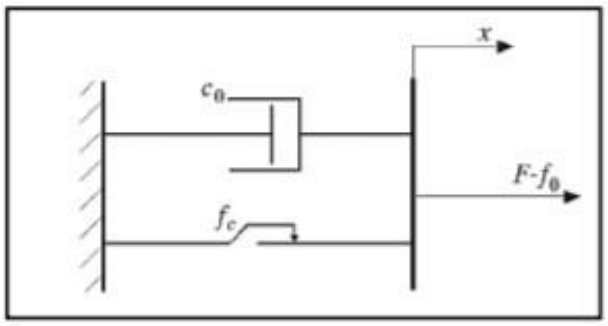

FIG. 14. Bingham model [21]

According to I. Mihai and F. Andronic (2014) and their research, the behaviors of the passive and active suspension system were analyzed using the MATLAB Simulink model. They concluded that the semi-active suspension total elimination of vehicle vibrations. The shape of the signal gives details on the strain induced in the spring. The damper stabilizes the vehicle. In case of huge disturbance, a semi-active suspension system eliminates the oscillation. This type can be employed in any vehicle to improve ride comfort and steering stability [22].

US Research Nanomaterials, Inc. (2013) in their publication "Nickel-Iron Oxide (NiFe2O4) - Properties, Applications" suggests the chemical properties, physical properties, and applications of the Nickel-Iron Oxide Nanoparticle. The application denotes that it finds a place in magnetic repulsive train levitation. This is a potential basic particle to build an MR Fluid with its excellent magnetic properties [23].

Joseph Scott Bunch in his paper suggested the physical and electrical behavioral properties of Graphene sheets. The structure, properties, behavior under different conditions were tested and explained. The graphene Sheets can be a great retaining particle due to their unique crystal structure. To obtain an MR Fluid whose structure contains a polymer chain-like structure that is present in an MR Elastomer might enhance the capacity of the MRF [24].

The potential advancement in the suspension industry has been in research for a decade to develop various improvements. Several pieces of research are being carried to validate different alternatives. As suspensions play a vital role in vehicle stability and safety, the experimental testing and validation required to evaluate the performance are done carefully. The parameters exhibited during testing are analyzed to determine the performance. Certain designs proposed by researchers have been experimentally and numerically verified to exhibit expected outcome performance. A research setup of a magnetorheological fluid damper was developed with a specifically formulated magnetorheological fluid to eliminate certain downsides commonly experienced with the conventional ones. The proposed design exhibited promising experimental results paving a way towards a future scope of converting the design into a product and some areas of research improvements [25]. This work focusses on further discussion of the background work and business analytics of the proposed design as a small-scale original equipment manufacturing (OEM) industry.

There several practices on building an industrial layout based on different parameters and processes involved in the manufacturing of the products. The layout built using the scope of JAVA called the

Computerized Relative Allocation of Facilities Techniques (CRAFT). The main aim of the implementation of these techniques is to obtain a facility layout having minimal material flow cost. The study was based on estimating the process step and the distance between the process station to determine a matrix to evaluate the best and most efficient layout to reduce the induced costs using a mathematical equation [26].

The aisle structures in a facility layout design have a huge role and affect the cost involved in the movement, time, and efficiency associated with the movement of materials and goods. The aisle structures must carefully analyze and designed considering different factors namely the usage of the entry and exits of a facility and its size, width, orientation, and so on. A mathematical model has been discussed and devised to determine the appropriate size, orientation, width, and several aisles in a particular facility to effectively use and cut down the wastes associated with it [27].

The facility layout design or industrial layout depends on numerous factors as indicated in different research. The parameters which decide on sustainable factors of the designed layout are termed as the sustainable facility layout which holds account of the social impacts such as the power consumed, pollution, and safety. These are discussed in detail for which a mathematical formula has been generated to determine the factor. This was built using numerous technologies such as big data analytics, machine learning, meta-heuristic which provide various data to analyze the sustainable compatibility of the layout [28].

A literature review of the parameters that drive the design of facility layout plan is studied and categorized based on the drivers. The study serves as a useful guideline tool for a designer as it guides and suggests some latest methodologies and their research to obtain data of process, method, and mathematical model [29].

The layout specifically customized to adopted for a foundry was proposed and studied to provide data on constraints and operation guidelines to cooperate with them [30]. There are several studies and predicting models to create a forecast of the adoption of innovative technologies in the market. In transportation and mobility sector are in research to develop CAM.

Many researchers have contributed towards predicting the outcome of these various technologies under different scenarios using different prediction models. Adoption of different latest technologies and their contribution towards enhancing the performance of autonomous vehicles are a constant area of research to scholars. A study was conducted using bass model to determine the adoption of autonomous truck for freight purpose[36]. The new car launch model and its sales prediction was carried out using previously launched similar model to evaluate the market statistics[37]. Different business models that are in use and their differences have been stated and discussed in this research to evaluate the electric vehicle adoption[40]. The research was dedicated to OEM manufacturing companies and the different business model and strategies to be adopted to capture market was discussed[41]. A review of the sustainable business models for automotive field was summarized[42]. A Delphi based scenario analysis to determine the most accurate business model for predict of automotive parts was covered in this research[43]. The development scope lying in the autonomous vehicle and its market has been analyzed and discussed by the author [44].

1.1. Evolution of suspension systems

The first used suspension arrangement consisted of a chain attached to the wheel frame which was later replaced with leather straps in carriages. However, this was upgraded to the leaf spring installed carriages to provide better life and endurance in the later 18th Century. In the Mid-19th century, elliptical springs were used as a suspension in carriages. The leaf springs were the first modern suspension that came into existence with the industrialization of acquired knowledge and skill a patent was filed. The coil springs were invented in the 20th century in a production vehicle, which is a conventional type of vehicle suspension to date. Later torsion bars, semi-independent and independent suspension systems came into usage with specific application-based vehicle design[1].

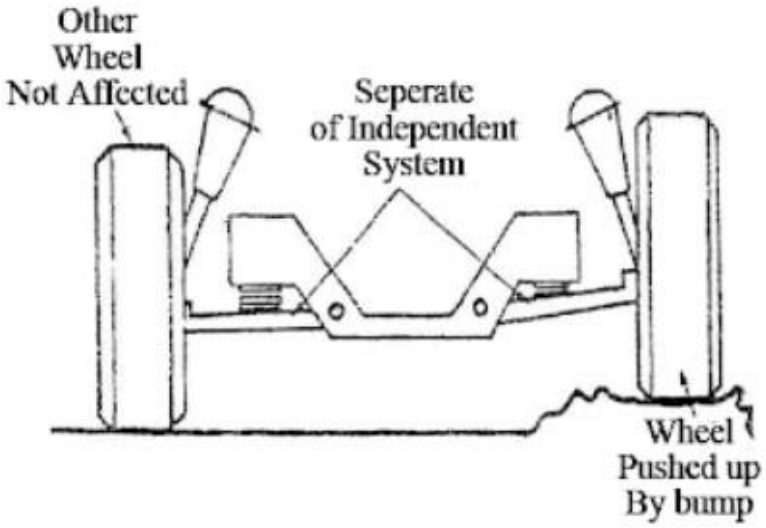

FIG. 15. Rigid or solid axle suspension[2]

The initial suspension designs were dependent on suspension mostly with rigid links to arrest and absorb the vibration. The Hotchkiss drive and torque tubes were the basic suspension designs in which the wheel movement of one was dependent on the other as they were rigidly connected that transmitted motion in one wheel to the another. These were used in typical applications like heavy carriages. With the need for individual wheel movement requirement came the design of an independent suspension system. In the independent suspension, each wheel is given an assembly that absorbs and arrests the transmit of motion from the road irregularity to the chassis. The early independent type suspension known is the leaf spring [1].

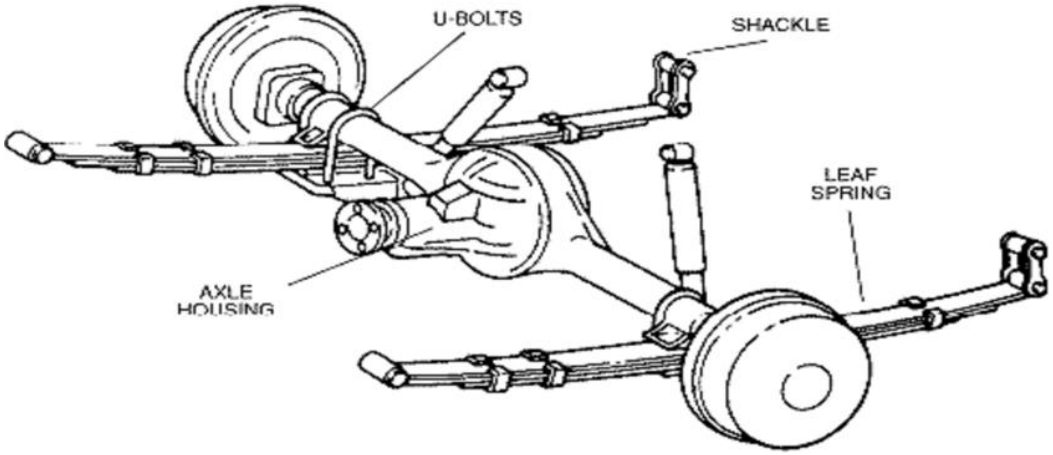

FIG. 16. Leaf spring suspension[3]

Evolution of the independent type suspension with the demand to increase performance and reduced size and weight in comparison to leaf spring brought coil or spring suspensions. The most used commercial suspension consists of a helical spring which provides the damping required to the vehicle in case of a bump or road irregularity and during cornering. Economical and commercial vehicles conventionally are installed with a spring-damper arrangement. The spring and damper arrangement consists of different components which constitute the different types in them namely: passive system, semi-active and active system, an interconnected system [1].

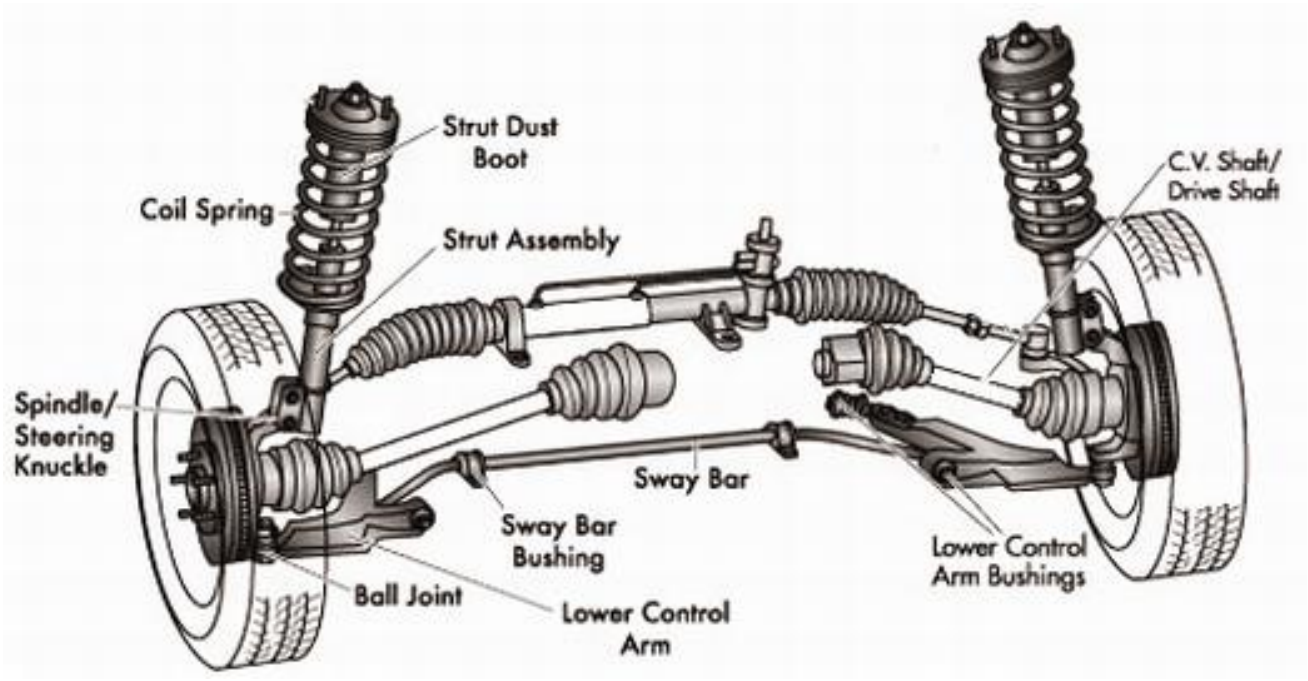

FIG. 17. Spring suspension assembly[3]

Types of spring suspension systems

The systems are assorted based on the capabilities delivered to the vehicle as a suspension as not all the systems offer the expected characteristics. Every suspension has a linkage, either pneumatic or hydraulic actuators' response. Based on the delivered characteristics of comfort quality and stability, they are classified as,[4]

1. Passive Suspension
2. Semi-Active Suspension
3. Active Suspension
4. Interconnected Suspension

In recent years the semi-active and active suspension have been potential areas of research serving a huge scope in overcoming the setbacks of the passive suspension to provide utmost characteristics aspects as a wholesome suspension system. We will briefly look into the characteristics of these different types [4].

1. Passive suspension

It comprises a damper filled with viscous liquid to provide damping and a coil spring of fixed stiffness to provide constant damping properties. They are simple in construction in comparison to the other types. They are reliable and inexpensive. The damper is a simple piston and cylinder arrangement that contains either a gas or a liquid that permits the free movement of the piston inside the cylinder while absorbing road abnormalities. The flow of liquid in the cylinder creates a force that is reactively proportional to the speed of sprung and unsprung masses. The coil stiffness retains the isolation of the absorbed energy from the chassis. Despite being a simple arrangement, It doesn't provide high stability as it lacks counteracting capabilities due to various reasons [4] .

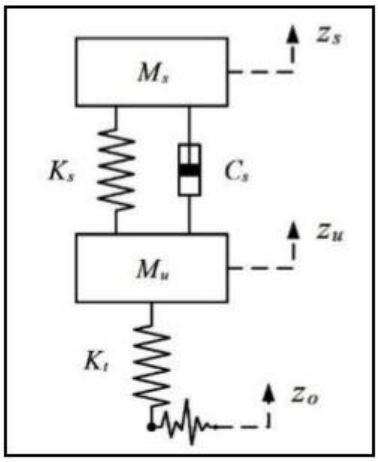

FIG. 18. Passive suspension system[4]

2. Semi active suspension

It provides variable damping to the system which is the same as in a passive system. The system can be adjusted to the required level of damping according to the environment to obtain smooth ride comfort. However, the spring stiffness remains constant. The change in damping coefficient can affect the energy

dissipation making it more convenient than a passive system. These can be controlled and adjusted either continuously or discontinuously using external forces or electrical energy to alter depending on the need. The adjusting capacity of this suspension type scores during critical cornering and braking and aids in avoiding chassis vibration and wheel resonance.

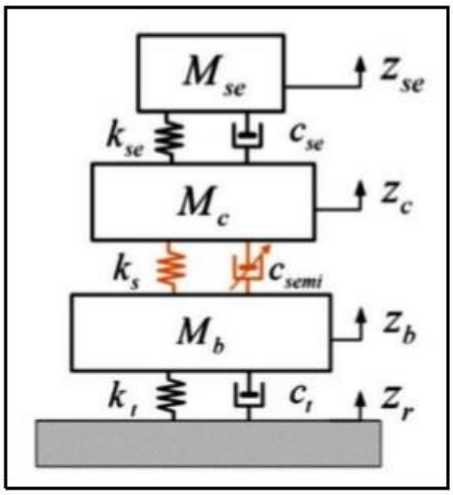

FIG. 19. Semi active suspension system[4]

3. Active suspension

This system consists of both mechanical and electrical devices integrated to adapt and control the damping concerning the given real-time signals. This system is made of an actuator that actuates by applying the active force depending on the various inputs from the sensors to determine the information to process a control algorithm. It can or cannot consist of a damper along with an actuator and a mechanical spring. This type of suspension has both springs and dampers actuated by an actuator depending on the variable vertical misalignments in the road with proper control methods. With this effective ride comfort and drive, handling can be achieved in comparison to the other types. These are usually installed inexpensive upgraded new generation cars due to their complexity and high cost inquired that directly provides high overall performance in the vehicle. The commonly designed active suspension systems contain either a hydraulic/pneumatic actuator or electromagnetic actuator[4].

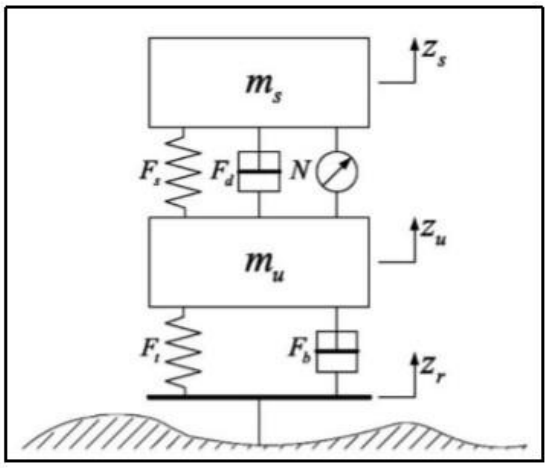

FIG. 20. Active suspension system[4]

3.1 Hydraulic/ Pneumatic Active Suspension

This type of active suspension has hydraulic/pneumatic actuators that are powered either by a battery or internal combustion engine. The hydraulic actuator is preferred over pneumatic for various reasons as they are simple in construction, easy to replace, high force density, reliability. This was employed in BMW's latest technology development by placing a rotary hydraulic actuator on the rear to maintain the anti-roll of the body. The disadvantages of hydraulic active suspension system need a continuous pressuring system, toxic hydraulic fluids affect environment, unfeasible space requirements [4].

3.2 Electromagnetic Active Suspension

This employs an electromagnetic actuator parallel to the spring arrangement to hold the mass of the vehicle. The electromagnetic actuator responds to the electrical signal which is given applied based on the control signal depending on the road conditions. This requires less power consumption in comparison to the hydraulic actuator. The advantages are increased efficiency, dynamic adaptability, stability, force control, dual operation. Whilst the disadvantages are space consumed by the system is high, higher current requirements, expensive[4].

4. Interconnected suspension

These systems have mechanical interconnections between them to decouple the mechanical vibrations in a vehicle in a passive manner. The connection can be hydraulic or pneumatic. An example of a mechanical interconnection is the anti-roll bars in vehicles. The hydraulic interconnections can offer great damping characteristics and flexibility providing stability. The interconnected hydropneumatic suspension was employed in Corolla 1996 model which denoted great handling while improvements can be made using a control system. The interconnected suspension system has been in research among academic researchers to determine their capabilities. It was employed using different gasses in later stages. The swing bar and anti-roll bars remain as simple interconnected mechanical systems [1].

Comparison

The different systems were analyzed, and respective qualities were assessed to determine the suitable. suspension system based on the priority of needs based on the application. They are tabulated as follows,

Table 1. Comparison of suspension types[4]

Parameters	Passive	Semi-Active	Hydraulic/Pneumatic Active	Electromagnetic Active	Interconnected
Structure	Simplest	Complex	Most complex	Simple	Simple
Weight/Volume	Lowest	Low	High	Highest	High
Cost	Lowest	Low	Highest	High	Medium

Ride Comfort	Bad	Medium	Good	Best	Good
Handling	Bad	Medium	Good	Best	Bad
Reliability	Highest	High	Medium	High	Good
Dynamic	Passive	Passive	Medium	Good	Medium

Recent advancements in suspension

1.Magnetorheological fluid dampers

The damper contains magnetorheological fluid that provides an adaptive damping coefficient depending on the road conditions. The magnetorheological fluid consists of magnetic particles such as ferrous or non-ferrous metal nanoparticles suspended in a fluid that responds to an applied magnetic field. This was invented by General Motors (GM), Now many companies have their formulation of the idea to compete. This area is an advancing field of research due to its huge potential to provide great ride handling capabilities coupled with maintained stability[5].

The quick adaptive response of this variant of suspension system completely relies on immediate interpretation of abnormalities and a control system to process this information to determine output. Various inputs are required to complete the control system to process the required action [5].

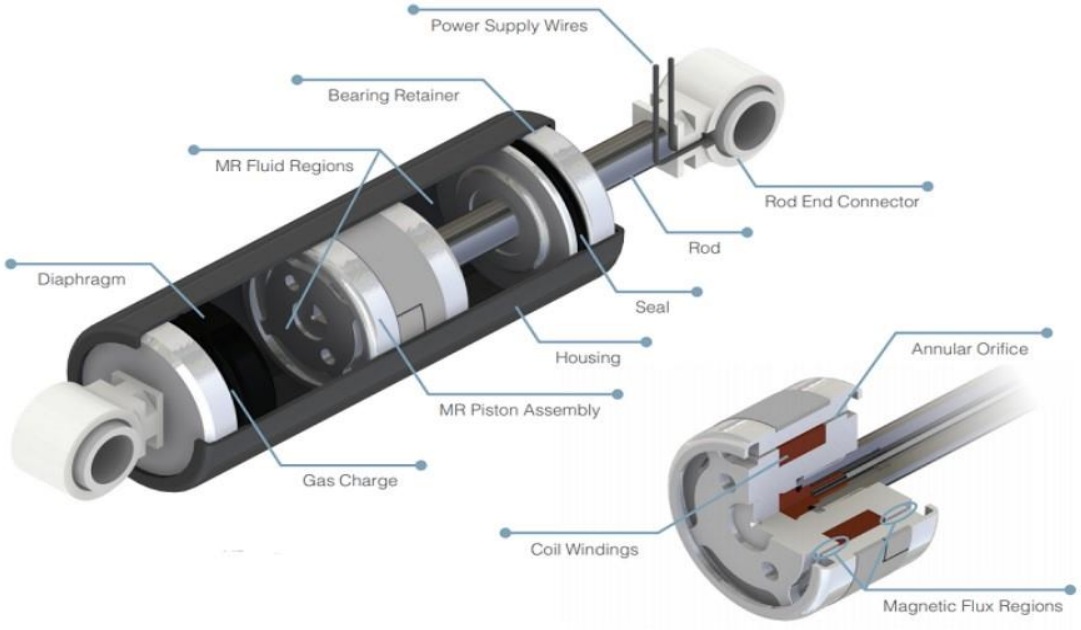

FIG. 21. Magnetorheological fluid damper[6]

2. Active curve tilting

This is the most recent advancement in integration with the scope of sensors employed in the vehicle proposed by Mercedes using lateral acceleration sensors with front-facing cameras to detect upcoming cornering and to adaptively tilt the air suspension to the apex. This mainly focuses on reducing the lateral

force on the passenger during cornering on poorly blanked corners on the road improving the ride quality [4].

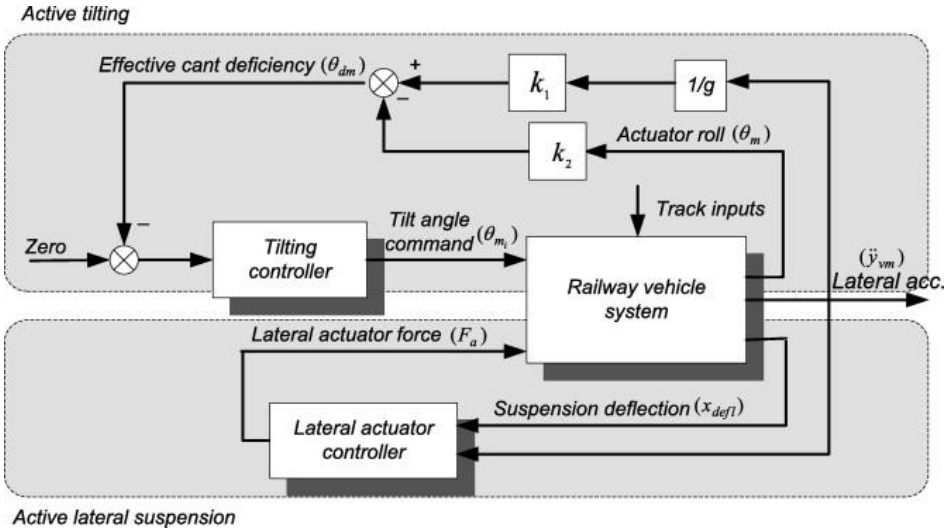

FIG. 22. Active curve tilt in railway vehicle control[7]

3. Hydraulic roll control

These employ a hydraulic system to transfer counterweight to balance body roll during driving conditions instead of the conventional steel rigid anti-roll bars. The hydraulic system would transfer the fluid to another end to counteract the weight and body roll. Vehicles with the best balance between handling and performance incorporate this system in various forms of approach to attain the output [4].

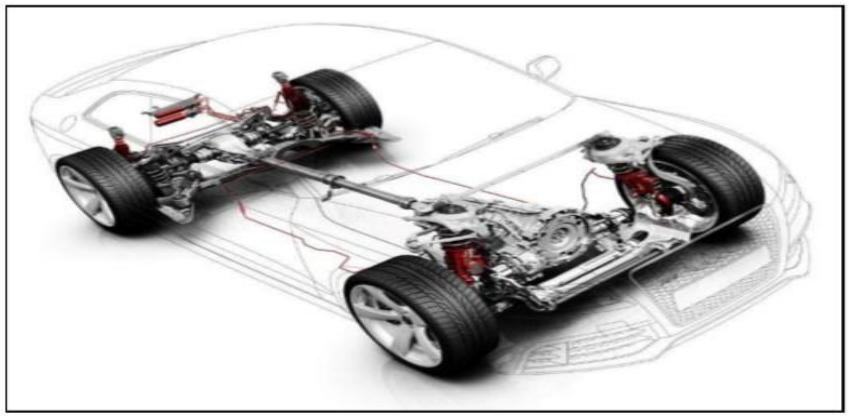

FIG. 23. Hydraulic roll control [4]

2. Magnetorheological fluid

Fluids that contain nano materials of magnetic responsive particles suspended in a carrier fluid that responds to applied magnetic field and transforms into a viscoelastic solid from a liquid state is called magnetorheological fluid in Fig. 24.

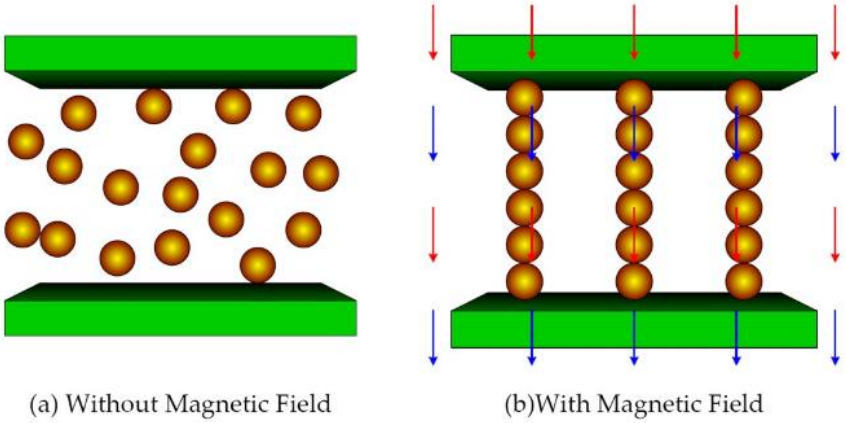

FIG. 24. Magnetic response of MR fluids[6]

The micro and nano particles in the fluid align themselves in the direction of the magnetic flux lines when a strong magnetic current or field is applied. The alignment of the particles changes the viscosity of the fluid instantly to behave as a shock absorbing semi solid.

2.1. Composition of the magnetorheological fluid

The composition and the concentration of the magnetorheological fluid were arrived at by the calculation of the damper specifications which were manufactured and scaled-down with actual dimensions to obtain the prototype scaled output performance measures of the behavior of the fluid. The elements of the proposed composition consist of the synthesized Nickel Iron Oxide, or Nickel Ferrite and Graphene suspended in silicone oil in which grease is added to achieve the viscous fluid consistency of the MR Fluid.

Table 2. Composition of the magnetorheological fluid

Sample	Nickel Iron Oxide + Graphene Composition	Silicone Oil Composition	Grease Composition
1	20% (7+1)	80% (32ml)	2.5 gms
2	25% (9+1)	75% (30ml)	2.5 gms
3	30% (11+1)	70% (25ml)	2.5 gms

The nickel ferrite or nickel iron oxide element is a ferromagnetic nano-sized particle that is responsible for contributing to the bas of the magnetorheological fluid in Fig. 25.

FIG. 25. Nano particles of nickel iron oxide

Graphene in Fig. 26 is the element that is expected to change the behavior of the particles in the liquid contributing the properties of enhanced magnetic response concerning the fatigue cycles of the magnetization experienced in dynamic conditions of the vehicle with the peculiar structure where carbon atoms retain their elemental space without colliding with one other, and the structure is never disrupted due to external forces on reasonable conditions. The sedimentation of the particles can also be avoided using Graphene to the composition due to its structure in Fig. 27.

FIG. 26. Graphene

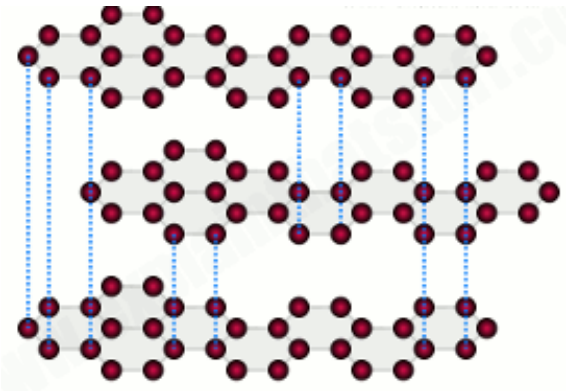

FIG. 27. Structure of graphene

Silicone oil in Fig. 28, is widely used carrier oil for various purposes. They have excellent temperature stability and good electrical transfer characteristics. The silicone oil is responsible for the fluidity and acts as the carrier liquid for the synthesized ferromagnetic nanoparticles of Nickel-Iron Oxide and Graphene. Grease in Fig. 29 It is added to retain the required quasi-liquid consistency of the MR fluid and to provide lubrication.

FIG. 28. Silicone oil

FIG. 29. Grease

2.2. Synthesis of nickel iron oxide

The Nickel Iron Oxide was prepared from Nickel Carbonate and Ferric Chloride substances. The Nickel Carbonate of molar weight 37.62 g of material was dissolved in 100 ml of distilled water to obtain one molar solution of the Nickel Carbonate. The Ferric Chloride of a molar weight 32.440 g of material was dissolved in 100ml of distilled water to obtain two molar solutions of Ferric Chloride.

FIG. 30. Alginic acid

The Alginic acid, in Fig. 30, acts as a binding agent for the composition to combine to form a completely combined solution containing both the Nickel and Iron ferromagnetic elements in them. The Alginic acid of 1 g is weighed and measured and dissolved in 50 ml of ammonia, and this solution is added to the prepared mixture of the Nickel Carbonate and Ferric Chloride solution to carry out the binding action.

FIG. 31. Triton X 100

The Triton X 100, in Fig. 31, acts as a surfactant and a buffer solution to the mixture. The mixed solution is stirred well and placed in a heater, in Fig. 32, and heated continuously for about 6-8 hours and stirred well until the water and moisture evaporate from the solution leaving behind the crystals of Nickel-Iron Oxide.

FIG. 32. Heating the nickel carbonate and ferric chloride solution

FIG. 33. Crystalline nickel iron oxide

The obtained crystalline Nickel Iron Oxide, in Fig. 33, was transferred into a crucible in Fig. 35, used to heat the component to high temperatures. The crucible containing the crystalline Nickel Iron Oxide is heated to high temperature of 300°C, 500°C, 700°C, and 900°C for 6 hours continuously in a muffle furnace in Fig. 34.

.

FIG. 34. Muffle furnace

After the completion of each temperature heating stage, the sample is taken out of the muffle furnace in crucible ground and crushed using a mortar and a pestle, in Fig. 35, 36 and the heating procedure is continued.

FIG. 35. Mortar and pestle

FIG. 36. Crucible

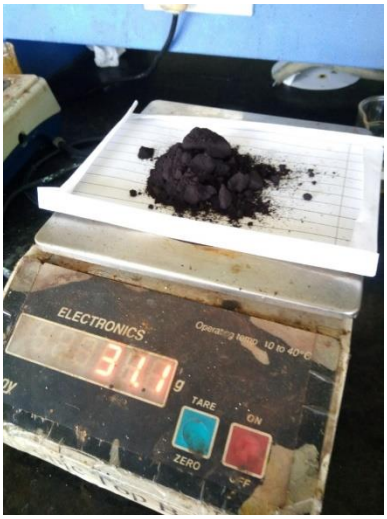

FIG. 37. Synthesized and weighted nickel iron oxide

The procedure was carried for the mentioned temperatures to obtain the nano-sized Nickel Iron Oxide particles after the grinding and churning process after every temperature cycle. The nanopowder or nanoparticles synthesized weighed about 31.1 g in Fig. 37.

2.3. Synthesis of graphene

The Graphene was synthesized, in Fig. 38 from reducing graphite by adding hydrogen peroxide. The graphite powder was measured and weighed of which 10 g was taken, and 10 ml of hydrogen peroxide was added and stirred. The obtained solution was heated until all the converted hydrogen molecules of water evaporated to form a clear fine powder of graphene, in Fig. 39.

FIG. 38. Graphite solution

FIG. 39. Synthesized graphene

2.4. Preparation of the fluid

The silicone oil is taken in a measuring beaker to measure the oil depending on the sample composition and pour it in a beaker with sample labels. A standard amount of 2.5 g of grease is added to each beaker for the respective samples. Initially, the silicone and the grease alone are stirred well to make a fluid with suiTable. fluidity and consistency. The measured weight of the nickel-iron oxide along with one gram of graphene is taken and added to the sample beaker respectively containing the silicone oil and grease fluid stirred using a magnetic stirrer, in Fig. 40.

FIG. 40. Magnetic stirrer

The sample containing all the elements is manually stirred well with a glass rod to remove clumps. The magnetic pellet is dropped in the prepared samples, and the beaker is kept on top of the base plate of the magnetic stirrer. The power supply is turned on, and the RPM magnetic pellet is set to the desired value. The rate of stirring contributes towards the dispersion of the nanoparticles in the fluid. The samples were

magnetically stirred, in Fig. 41, for about 6 hours at normal temperature to obtain the complete and proper dispersion of the particles.

FIG. 41. Magnetic stirring of the MRF

The samples were then collected in glass bottles with sample labels for identification. These samples were then kept in a sonicator, in Fig. 42, to achieve complete dispersion of solid particles in the liquid.

FIG. 42. Ultra sonicator

2.5. Magnetorheological fluid damper

The fabricated MR damper as in Fig. 43 setup consists of the following parts which are assembled as a damper setup for the testing purpose. The parts are

1. Cylinder,
2. Cylinder Head,
3. Piston Rod,
4. Piston Head,
5. Coil Windings
6. Base Plate

Table 3. Dimensions of fabricated MRF damper

Cylinder	Cylinder Head	Coil Winding	Piston Rod	Piston Head
a. Diameter =46 mm b. Inner Diameter = 40 mm c. Overall Length = 97 mm d. Thickness = 3 mm e. Thread length = 17 mm f. Nylon sleeve diameter = 44 mm g. Metal sleeve diameter = 42 mm	a. Outer Diameter = 46 mm b. Inner Diameter = 44 mm c. Length = 34 mm d. Hole Diameter = 22 mm e. Thread length = 17 mm	a. Number of turns = 432 turns (216 turns in each step) b. The thickness of the coil =0.315 mm (as per SWG scale) c. Maximum allowable current = 5 amps d. Maximum allowable voltage = 12 volts	a. Diameter = 22 mm b. Length = 125 mm c. Thread length = 13 mm d. Hole(at the top)=6 mm e. Hole (at the bottom) = 3 mm	a. Diameter, D1 = 30 mm b. Diameter, D2 = 22 mm c. Length = 37 mm d. Number of steps = 2 e. Thickness of each step = 5 mm f. Distance between two steps = 11 mm g. Hole depth = 30 mm h. Hole diameter (for thread) =9 mm i. Number of grooves= 4

The damper testing consists of a setup that includes various components namely the quarter car model, power amplifier, data acquisition card, accelerometer, regulated DC power supply, vibration shaker machine, cooling system, and a system with LABVIEW software.

FIG. 43. Fabricated damper

2.6. Damper calculations

Volume of cylinder$= \pi r^2 h$

$= \pi * 202 * 80$

$= 100{,}480\ \text{mm}^3$

$= 100{,}480\ \text{ml}$

Volume of damper$= \pi r^2 h$

$= \pi * 152 * 37$

$= 26{,}140.5\ \text{mm}^3$

$= 26.14\ \text{ml}$

Volume of MR fluid = Volume of Cylinder – Volume of Damper
= 100.48 - 26.14
= 74.34 ml
However, only half the damper must be filled with MR fluid.
Therefore, 37.17 ml of fluid is required.

2.7. Damper testing equipment

The damper testing consists of a setup that includes various components namely the quarter car model, power amplifier, data acquisition card, accelerometer, regulated DC power supply, vibration shaker machine, cooling system, and a system with LABVIEW software.

The quarter car model consists of a setup to house the damper, in Fig. 44, in a similar manner in which the damper will be installed in an automobile vehicle. It consists of a base plate, top plate, and guide rods which are assembled to accommodate the damper between the base and the top plates which are guided by the guide rods and held in place by springs inserted into the guide rods. The base plate has drilled holes on which the base plate of damper is placed and fastened with fasteners. The guide rods are attached to the base plates by the three drilled holes for the guide rods. The springs are inserted into the guide rods and the top plate is inserted. The damper piston is held upright and fastened below and above the top plate to hold its position.

A sprung mass of 12 kg is considered a standard weight to assess the performance of the damper. This weight is positioned on top of the top plate and fastened to hold and grip this weight in place during the testing procedure. The whole setup is mounted on the vibration plate which is fastened to the vibration shaker machine. The vibration plate and the base plate of the quarter car model have fastened in such a manner that the vibration plate excites the complete setup providing the necessary disturbance required to test the damper, in Fig. 44.

FIG. 44. Damper mounted on the Quarter car model in the vibration shaker

The power amplifier, in Fig. 45, is the system that gives variable inputs to the vibration shaker to control the output level, frequency, and range of vibration. The input values of the frequency, output level, and range are varied to feed the value to the shaker to excite the setup.

FIG. 45. Power amplifier

The signal input from the power amplifier controls the excitation of the setup in the vibration shaker and the output performance of the setup corresponding to the exciting frequency is acquired from the accelerometer and data acquisition card along with LABVIEW Signal Express software.

An accelerometer, in Fig. 46, is a device that measures the motion of a structure. It is connected to the top and base plate to acquire signals corresponding to the applied frequency to set up.

FIG. 46. Accelerometer

Data acquisition card, in Fig. 47, is used to alter analog waveforms into digital values for processing. The data acquisition card has the accelerometer connected to one of its ports, via a wire. Another wire connects the card with one of the USB port sofa computers. Software programs control data acquisition applications.

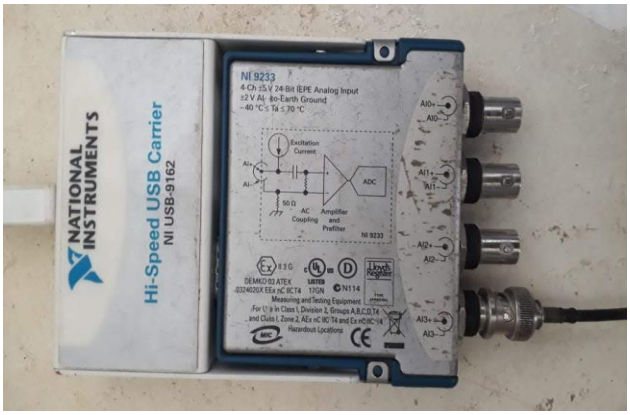

FIG. 47. Data acquisition card

LABVIEW (short for Laboratory Virtual Instrumentation Engineering Workbench), in Fig. 48, is a signal processing software used to convert the signals captured using accelerometer into waveforms of displacement to understand the motion of the top plate. The vibrations produced in the quarter car setup can be recorded using LabVIEW software. It is used to gain the signals corresponding to the set frequency which can be recorded and analyzed to acquire the acceleration and displacement changes in the setup.

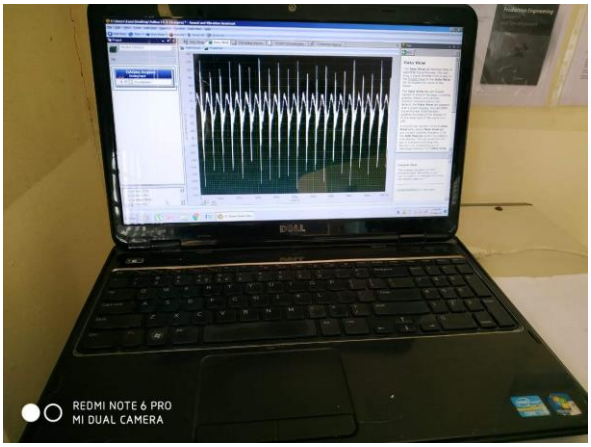

FIG. 48. LABVIEW signal express software

Regulated DC Power Supply, in Fig. 49, is a device that varies the voltage and current applied. A regulated power supply is a circuit that translates unregulated AC (Alternating Current) into a constant DC. It uses a rectifier to convert AC supply into DC. Its function is to supply a stable. voltage. It is coupled to the damper to vary the input voltage to obtain the performance at different levels of voltage input.

FIG. 49. Regulated DC power supply

Electrodynamic Shaker, in Fig. 50, produces vibration based on the principle of magnetism. It is either air-cooled or water-cooled.

FIG. 50. Vibration shaker

This is used to stimulate the setup mounted on the vibration plate and it is controlled by the power amplifier for the frequency and operating range for the output level. An air-cooled shaker, in Fig. 51, features a centrifugal blower for forced air cooling. A hosepipe connects the bottommost of the shaker to the blower which sucks air from a perforated sheet at the highest of the shaker.

It is very vital to confirm that the blower is not located in close vicinity of the shaker because this might cause the exhaust air from the blower to be sucked back by the shaker. In this scenario, the shaker's temperature will keep increasing as it is being cooled by the same air in a loop, causing thermal runaway and even burning of the armature coil.

To ensure safety and proper operation of the cooling system, various sensors are installed in the shaker that is mentioned below:

1. Air Pressure Sensor – To ensure sufficient air pressure for proper suction.
2. Air Temperature Sensor – To stop the system if the air temperature is too high to ensure proper cooling.

Due to suction, audible noise is always present near the shaker and the blower. It is suggested to take measures during installation to prevent this audible noise from creating an un-conductive working environment for the test/ lab personnel.

FIG. 51. Vibration shaker cooler

2.8. Damper testing procedure

The following steps are carried out to test the damper in the apparatus,

1. The vibration shaker machine cooler is turned on and the cooler is allowed to run for about 5 minutes before the vibration shaker is excited to avoid the damage of the coil in the vibration shaker.
2. The accelerometer is fixed to the base plate and the frequency of excitation is varied from 2Hz-20 Hz in steps of 2 with an output level of 8.
3. The vibration signal is acquired and captured using the accelerometer and DAQ using the LABVIEW Signal Express Software.
4. To capture the signal, open the LABVIEW Signal Express Software, Sound and Vibration, Select the file and go to New Project and select Save to save the project.
5. Click on Add step, select acquire signals, select DAQ to acquire, select analog, and select acceleration.
6. In the popup menu enter the numerals of the sensitivity of the accelerometer, sample read values, and the unit in which the data should be acquired.
7. Now, click on Data view, select Run to play the acquiring signal from the accelerometer.
8. Now using the power amplifier, the frequency and the output level are changed and set to the required value and the acquiring signal is recorded by selecting Record by entering the file name to save the recording and then Stop to abort the action in Fig. 52.
9. Then, for each value of the frequency, the same procedure is carried to acquire and record the signal for the base plate readings. The recordings are displayed in the history dialogue box below.
10. Later, the accelerometer is placed on the top plate and the same procedure is repeated to acquire the top plate readings.
11. Now, the input voltage is given to the damper in steps of 5 for the range of 5 V-20 V for which the frequency range is 2 Hz-20 Hz varied in the steps of 2 to acquire 40 signal readings of each voltage summing to a total of 120 readings by following the same test procedure.

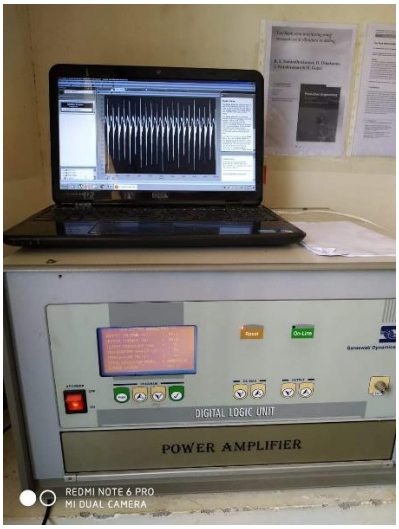

FIG. 52. Recording of vibration signals

2.9. Signal analyzing procedure

The following steps are carried out to test the damper in the apparatus,

1. The LABVIEW Signal Express Software, Sound, and Vibration is opened, and the project is retrieved to view all the acquired data.
2. Select on Monitor/Record and change to Playback mode and then, select the signal to be analyzed from the list of acquired signals and run the signal.
3. Click on Add step, Select Load/ Save signal, click on Analog, select Save to ASCII, select on browse to select the location to save the data file, change the options to Append to file and Generic Text File and then Run the signal to save the recorded data.
4. Now, Click on Add Step, Select Load/Save signal, Select Load from ASCII, Select browse and obtained the save text data file for the analyzing signal saved in the previous step.
5. The data generated from the signal is copied to the analyzing column area, Now click on Import segments, Change the None option to the column to and copy the user data value.
6. Now, select both the Columns on the dialogue box and allow the option to change to none and unselect column 1 and paste the user dt value to change the signal corresponding to the recording time.
7. Change the Voltage option to Acceleration.
8. Now, Click on Add Step, Select Analyze, Click on Timed Domain, Select Vibration Level to display the acceleration signal for the recorded time of the analyzed signal.
9. Record the RMS Acceleration values of the obtained signal and tabulate for the later purpose to plot graphs to analyze, in Fig. 53.

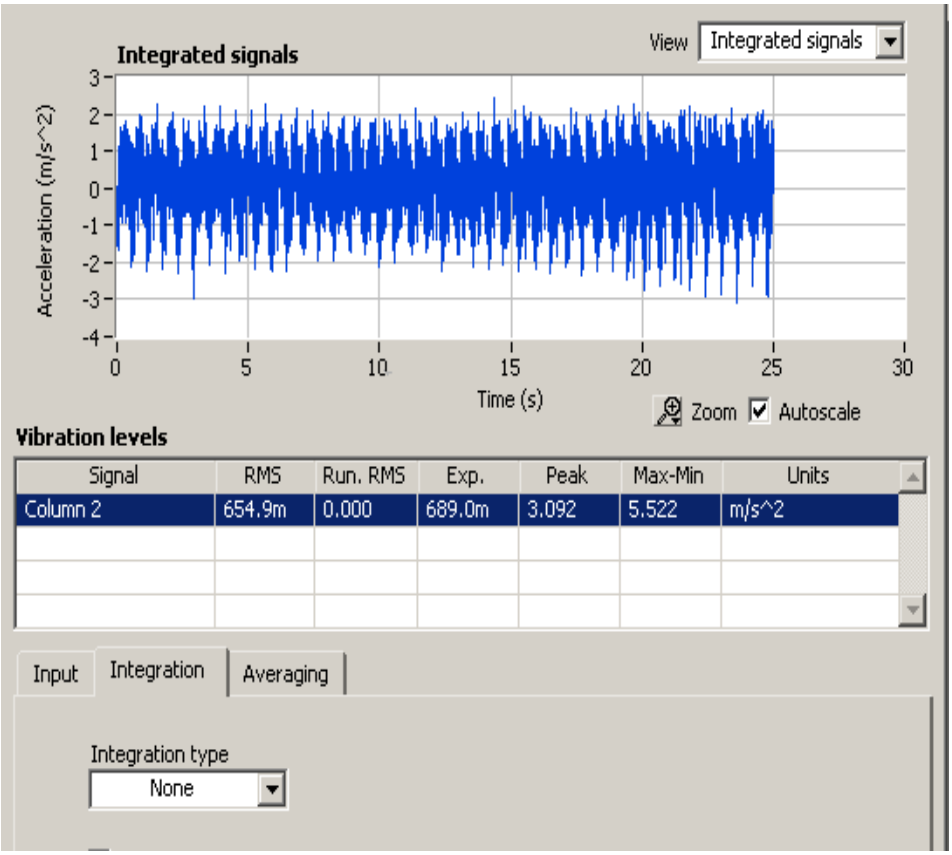

FIG. 53. RMS acceleration values

10. Now, click on the None option and select the Double Integrate option to obtain the values of displacement for the analyzed signal.
11. Similarly, the RMS Displacement values are tabulated, in Fig. 54.
12. The same procedure is carried out for every of the acquired signals and analyzed to obtain the acceleration and displacements values for the comparison of the output performance of the samples concerning applied frequency and voltage

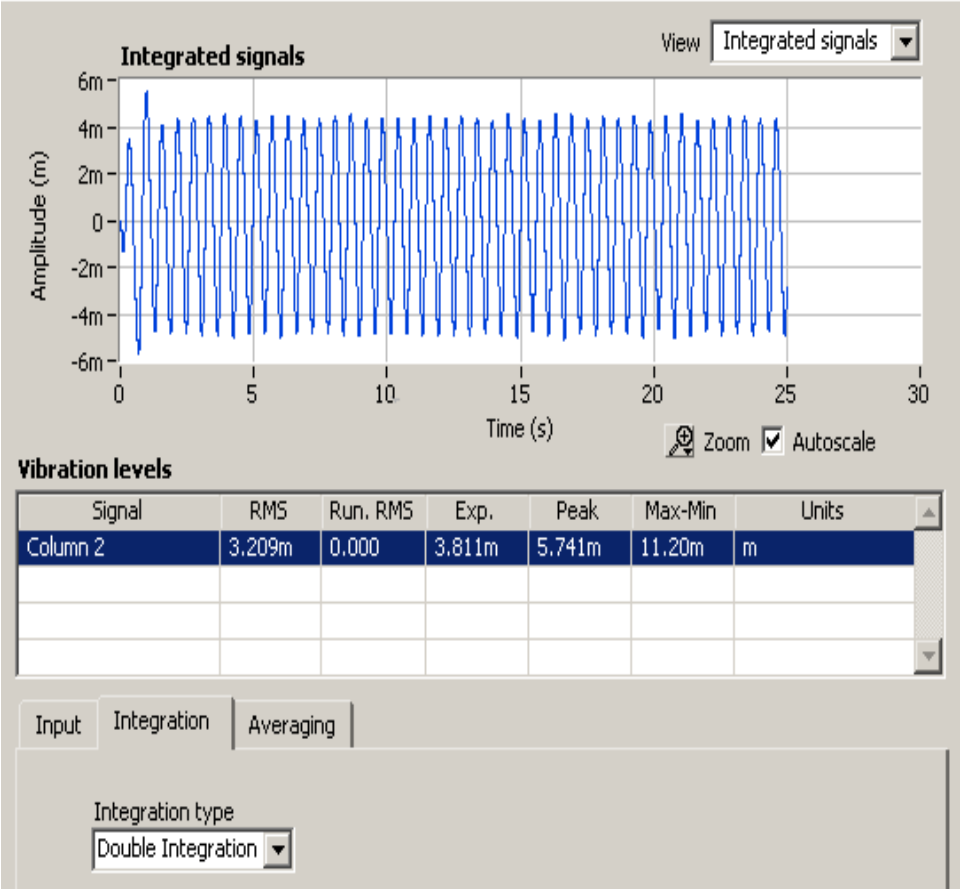

FIG. 54. RMS displacement values

2.10. Particle and Fluid Property Analysis

The synthesized nickel oxide particles were observed under a scanning electron microscope (SEM) to evaluate and understand the particle size, arrangement, and shape. The observation was done to determine the properties exhibited by the nickel oxide particles when a magnetic field is induced. The fluid samples containing the dispersed particles at different concentrations were subjected to rheometer testing to analyze and study the rheological characters of the fluid under ambient conditions keeping information from hysteresis of MR fluid study as a reference [9]. The fluid behavior of non-Newtonian fluid samples can be determined with the obtained results.

1. Scanning Electron Microscope

The specimen being a non-biological component, the accelerating voltage was maintained at a constant at 20 kilovolts (kV) and the magnification of the image was increased at each step. The images were captured at x10000, x20000, x30000, x55000 in Fig. 55 (a),(b),(c),(d). The images prove that the magnetic elements are in a polydisperse state where both micro and nanoparticles of nickel oxide coexist. The coexistence of nano and microparticles in an MR fluid has significant benefits. The exhibited structure can greatly eliminate the hard cake formation of these particles when subjected to periodic magnetization as a magnetic particle suspended in MR fluid as indicated in a previous study. [14]

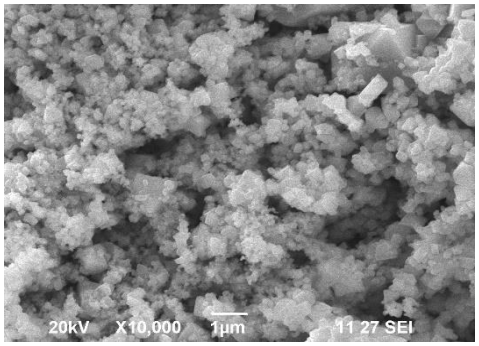

Fig. 55 (a)

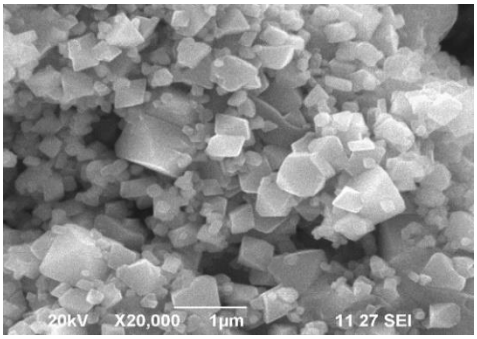

Fig. 55 (b)

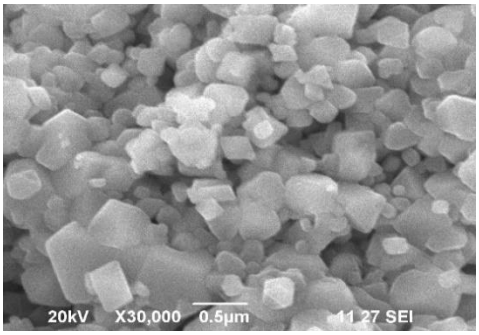

Fig. 55 (c)

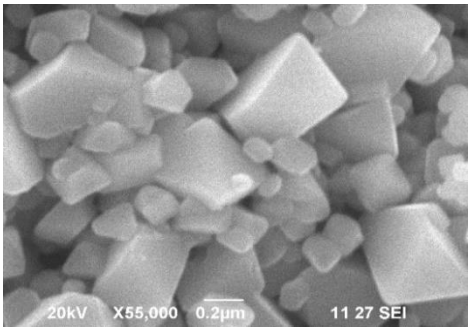

Fig. 55 (d)

FIG. 55. (a),(b),(c),(d) SEM images of synthesized nickel oxide

2. Rheometer

Rheometers are devices used to obtain the rheology of fluids. The process that comprises the study of behavioral changes of fluid to applied forces is called rheology. Rheometers are of two types: shear and extensional rheometers. The parallel plate shear geometry rheometer was used to obtain shear stress, shear strain, the viscosity of the fluid at a constant rotational speed of the plates concerning time.

FIG. 56. Rheometer

A graph of the required data was obtained from which the exact numerical data can be arrived at and tabulated. The values are plotted as a graph against the analyzing parameters. The association between the shear stress and shear rate for the studied samples at 25°C obtained from different shearing times, under increasing and decreasing incline in shear stress in Fig.. 56. It should be

remembered that the shear flow curve under the rising incline in shear stress is greater in all samples than that obtained under the decreasing ramp. During the increasing ramp in shear stress, the structure and the flocculants of the fluid breaks down and decrease further when the shear stress is increased in graphs Fig. 57. Conversely, lowering the stress rate during the reverse process will induce flocculant growth and allow the particulate network to recover the expanded stress spectrum examined, suggesting that the fluid was stable. during the experimental study. The increasing stress range investigated, indicates that the fluid was stable. during the experimental work. The fluid behavior was close to a Newtonian fluid.

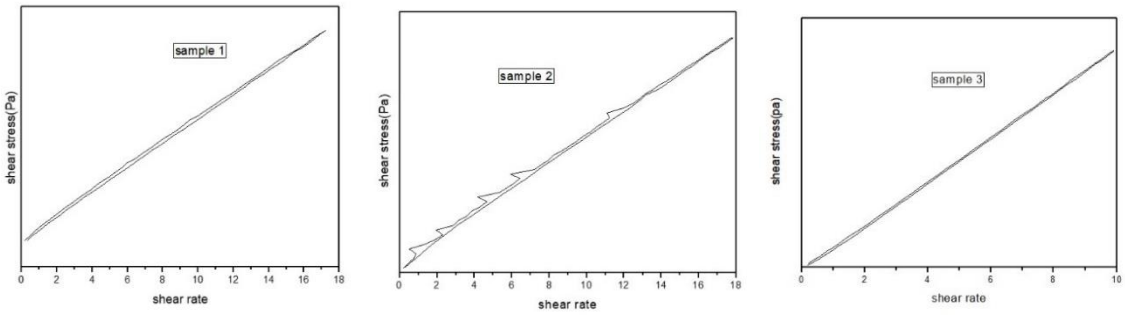

FIG. 57. Shear stress Vs Shear rate of sample 1,2,3

2.11. Vibration analysis of damper

The obtained data of the acceleration and displacement for the different conditions of the applied voltage and applied vibration frequencies are tabulated according to the different conditions of the analysis to be carried out. The values of the acceleration and displacements were grouped separately for the applied voltage conditions and for each sample to evaluate and validate the output performance achieved at the applied conditions of voltage and vibrations. The acceleration data for the 5 V input were obtained for the samples and were tabulated, Table. 4 along with base readings to plot the graph, Fig. 58 of the output performance of acceleration for each sample. The graph was plotted with tabulated values of acceleration for 5 V for each sample taking the applied frequency on the X-axis and the acceleration values on the Y-axis denoting the vibrating acceleration of the top plate concerning the applied voltage.

Table 4. Acceleration for 5 V (m/s^2)

Frequency (Hz)	Base	Sample 1	Sample 2	Sample 3
2	0.645	1.501	0.987	2.269
4	61.6	48.96	2.827	7.641
6	12.46	12.27	7.641	10.46
8	8.841	7.385	11.29	8.469
10	7.72	7.86	10.89	7.145
12	9.553	7.473	10.16	7.619
14	7.944	7.71	11.02	6.727

16	9.594	8.508	9.94	7.739
18	11.03	10.37	9.782	8.072
20	9.3	11.24	13.1	9.616

The graph denotes that the acceleration of the vibrating top plate is reduced considerably for all the samples. The range of the difference in the acceleration of the vibrating top plate is 16.66% to 91.66% concerning the base readings obtained. The highest vibration damping for the 5 V input voltage is obtained with sample 2. The steady output for arresting the excitation of the top plate for the entire frequency range is achieved in sample 3 for 5 V input voltage.

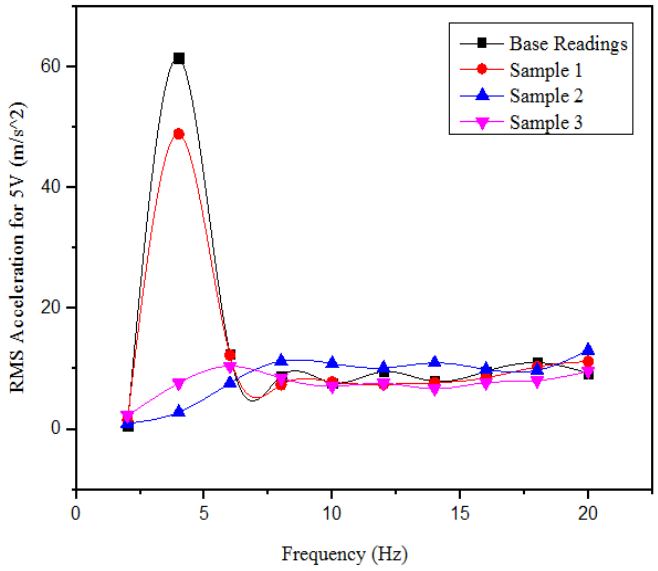

FIG. 58. Acceleration for 5 V

The acceleration data for the 10 V input were obtained for the samples and were tabulated, Table. 5 along with base readings to plot the graph, Fig. 59 of the output performance of acceleration for each sample. The graph was plotted with tabulated values of acceleration for 10 V for each sample taking the applied frequency on the X-axis and the acceleration values on the Y-axis denoting the excitation acceleration of the top plate concerning the applied voltage.

Table 5. Acceleration for 10 V (m/s^2)

Frequency (Hz)	Base	Sample 1	Sample 2	Sample 3
2	0.645	10.02	8.12	2.041
4	61.6	10.04	8.745	4.724
6	12.46	10.05	11.33	9.855
8	8.841	10.12	11.47	9.584
10	7.72	7.882	10.07	9.429

12	9.553	8.086	10.72	8.932
14	7.944	8.019	12.56	10.23
16	9.594	10.23	10.46	10.03
18	11.03	6.816	11.23	10.7
20	9.3	7.165	8.064	9.611

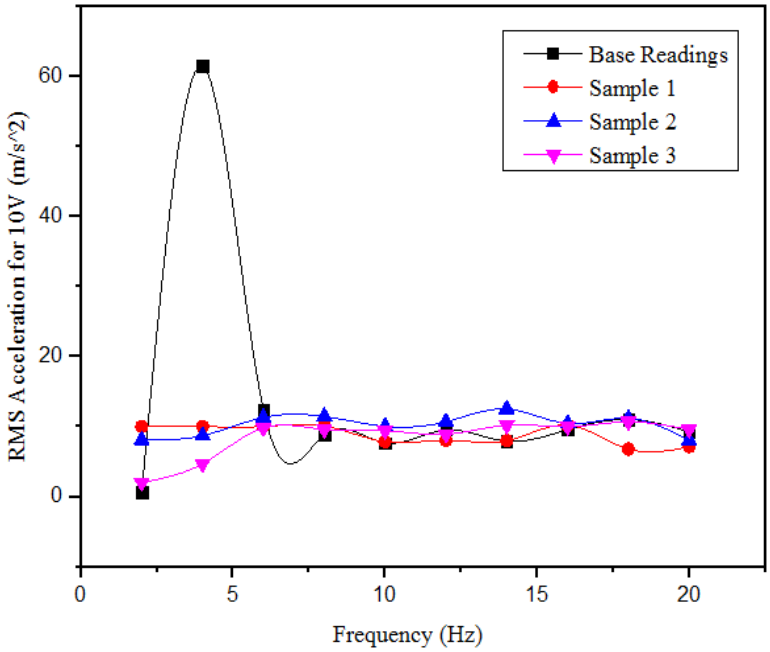

FIG. 59. Acceleration for 10 V

The graph denotes that the acceleration of the vibrating top plate is reduced considerably for all the samples. The range of the difference in the acceleration of the vibrating top plate is 83.33% to 91.66% concerning the base readings obtained which denotes the high output performance of reducing the vibration at the higher efficiency range. The highest vibration damping for the 10 V input voltage is obtained with sample 3. The steady output for arresting the vibration of the top plate for the entire frequency range is achieved in sample 2 for 10 V input voltage.

The acceleration values for the 15 V input were obtained for the samples and were tabulated, Table. 6 along with base readings to plot the graph, Fig. 60 of the output performance of acceleration for each sample. The graph was plotted with tabulated values of acceleration for 15 V for each sample taking the applied frequency on the X-axis and the acceleration values on the Y-axis denoting the vibrating acceleration of the top plate concerning the applied voltage.

Table 6. Acceleration for 15 V (m/s^2)

Frequency (Hz)	Base	Sample 1	Sample 2	Sample 3
2	0.645	1.499	0.702	0.942
4	61.6	71.91	10.46	4.987
6	12.46	8.479	14.29	9.188
8	8.841	8.8267	11.12	8.007
10	7.72	10.63	9.54	6.862
12	9.553	9.953	9.842	6.56
14	7.944	8.033	8.718	8.719
16	9.594	9.135	10.42	7.644
18	11.03	9.408	8.2	7.644
20	9.3	9.178	6.689	7.947

The graph denotes that the acceleration of the vibrating top plate is reduced considerably for all the samples. The range of the difference in the acceleration of the vibrating top plate is 80% to 91.66% concerning the base readings obtained. The highest vibration damping for the 15 V input voltage is obtained with sample 3. The steady output for arresting the vibration of the top plate for the entire frequency range is achieved in sample 3 for 15 V input voltage. The acceleration values for the 20 V input were obtained for the samples and were tabulated, Table. 6 along with base readings to plot the graph, Fig. 60 of the output performance of acceleration for each sample.

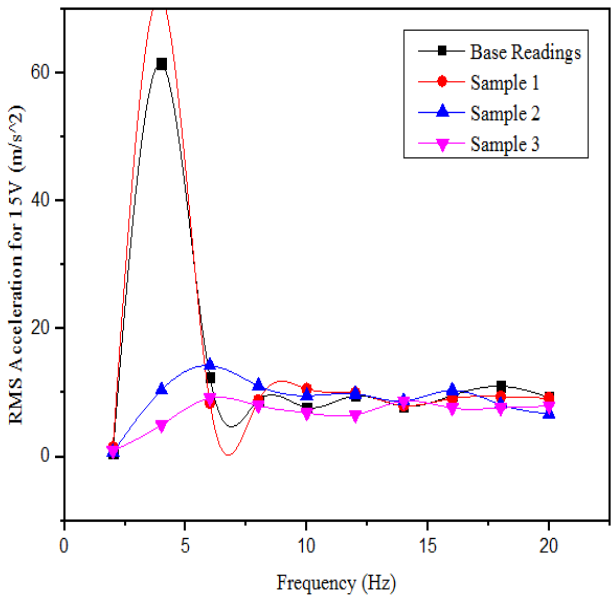

FIG. 60. Acceleration for 15 V

Table 7. Acceleration for 20 V (m/s^2)

Frequency (Hz)	Base	Sample 1	Sample 2	Sample 3
2	0.645	0.771	1.869	1.284
4	61.6	58.39	11.75	7.178
6	12.46	12.39	9.158	9.644
8	8.841	14.07	10.16	7.13
10	7.72	14.33	8.26	6.693
12	9.553	12.32	8.133	6.422
14	7.944	10.58	9.935	6.959
16	9.594	11.21	10.15	8.166
18	11.03	11.92	10.15	8.308
20	9.3	11.5	8.835	8.212

The graph was plotted with tabulated values of acceleration for 20 V for each sample taking the applied frequency on the X-axis and the acceleration values on the Y-axis denoting the vibrating acceleration of the top plate concerning the applied voltage. The graph denotes that the acceleration of the vibrating top plate is reduced considerably for all the samples. The range of the difference in the acceleration of the vibrating top plate is 3.33% to 91.66% concerning the base readings obtained. The highest vibration damping for the 15 V input voltage is obtained with sample 3. The steady output for arresting the vibration of the top plate for the entire frequency range is achieved in sample 3 for 15 V input voltage.

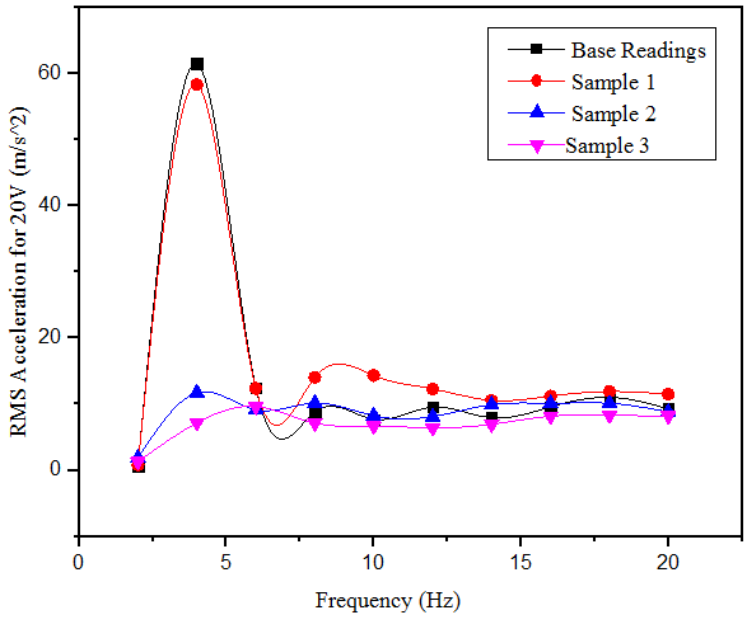

FIG. 61. Acceleration for 20 V

The acceleration values for sample 1 were obtained by varying the input voltage and frequency for which the values were tabulated, Table. 8 along with base readings to plot the graph, Fig. 62 of the output performance of acceleration. The graph was plotted with tabulated values of acceleration for sample 1 taking the applied frequency on the X-axis and the acceleration values on the Y-axis denoting the vibrating acceleration of the top plate concerning the applied voltage. The graph denotes that the acceleration of the vibrating top plate is reduced considerably at different input voltage. The vibrations are arrested at a higher voltage at a high frequency of vibration.

Table 8. Acceleration of sample 1

Frequency (Hz)	5 V	10 V	15 V	20 V
2	1.501	10.02	1.499	0.771
4	48.96	10.03	71.91	58.39
6	12.27	10.05	8.479	12.39
8	7.385	10.12	8.8267	14.07
10	7.86	7.882	10.63	14.33
12	7.473	8.086	9.953	12.32
14	7.71	8.019	8.033	10.58
16	8.508	10.23	9.135	11.21
18	10.37	6.816	9.408	11.92
20	11.24	7.165	9.178	11.5

Due to the resonant conditions of the test apparatus at low frequency the acceleration of the plate is high. The steady output of damping of the vibration is achieved at 10 V for Sample 1.

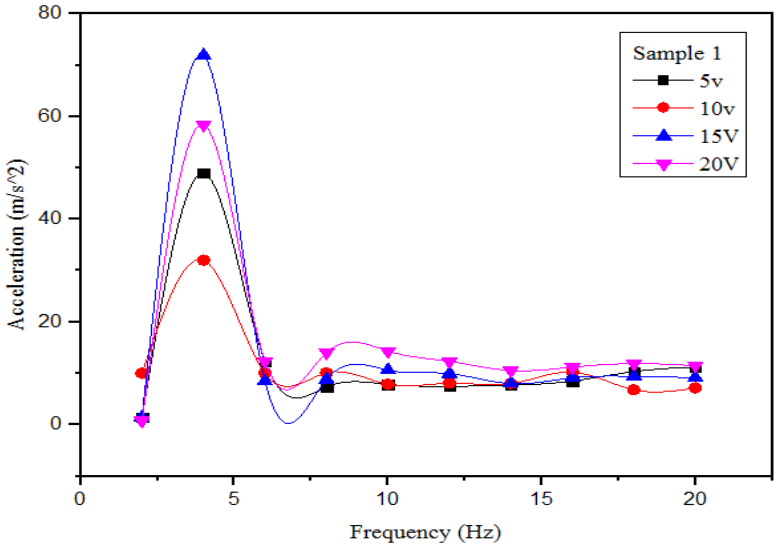

FIG. 62. Acceleration of sample 1

The acceleration values for sample 2 were obtained by varying the input voltage and frequency for which the values were tabulated, Table. 9 along with base readings to plot the graph, Fig. 63 of the output performance of acceleration.

Table 9. Acceleration of sample 2

Frequency (Hz)	5 V	10 V	15 V	20 V
2	0.987	8.12	0.702	1.869
4	2.827	7.845	10.46	11.75
6	7.641	11.33	14.29	9.158
8	11.29	11.47	11.12	10.16
10	10.89	10.07	9.54	8.26
12	10.16	10.72	9.842	8.133
14	11.02	12.56	8.718	9.935
16	9.94	10.46	10.42	10.15
18	9.782	11.23	8.2	10.15
20	13.1	8.064	6.689	8.835

The graph was plotted with tabulated values of acceleration for sample 2 taking the applied frequency on the X-axis and the acceleration values on the Y-axis denoting the vibrating acceleration of the top plate concerning the applied voltage.

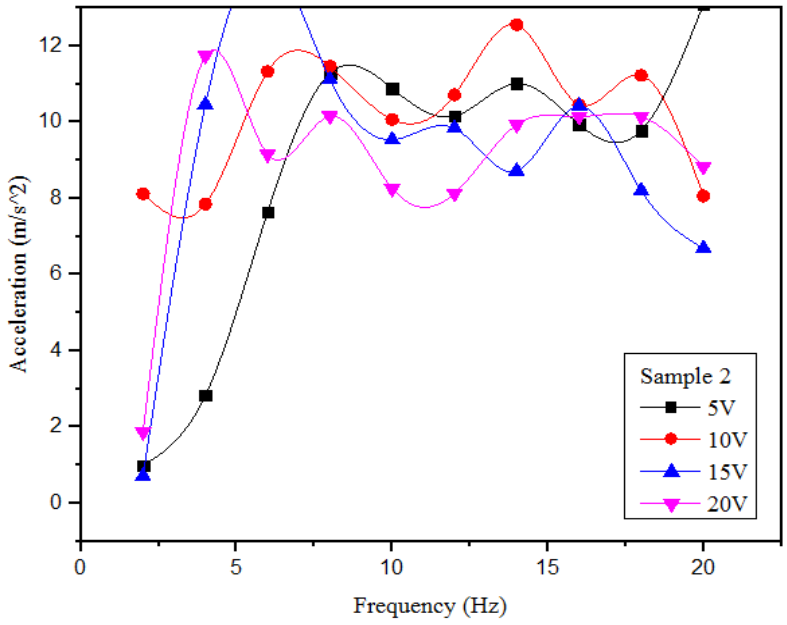

FIG. 63. Acceleration of sample 2

The graph denotes that the acceleration of the vibrating top plate is reduced considerably at different input voltage. The vibrations are arrested at a higher voltage at a high frequency of vibration. Due to the resonant conditions of the test apparatus at low frequency the acceleration of the plate is high. The steady output of damping of the vibration is achieved at 10 V for Sample 2.

The acceleration values for sample 3 were obtained by varying the input voltage and frequency for which the values were tabulated, Table. 10 along with base readings to plot the graph, Fig. 64 of the output performance of acceleration. The graph was plotted with tabulated values of acceleration for sample 3 taking the applied frequency on the X-axis and the acceleration values on the Y-axis denoting the vibrating acceleration of the top plate concerning the applied voltage.

Table 10. Acceleration of sample 3

Frequency (Hz)	5 V	10 V	15 V	20 V
2	0.987	8.12	0.702	1.869
4	2.827	7.845	10.46	11.75
6	7.641	11.33	14.29	9.158
8	11.29	11.47	11.12	10.16
10	10.89	10.07	9.54	8.26
12	10.16	10.72	9.842	8.133
14	11.02	12.56	8.718	9.935
16	9.94	10.46	10.42	10.15
18	9.782	11.23	8.2	10.15
20	13.1	8.064	6.689	8.835

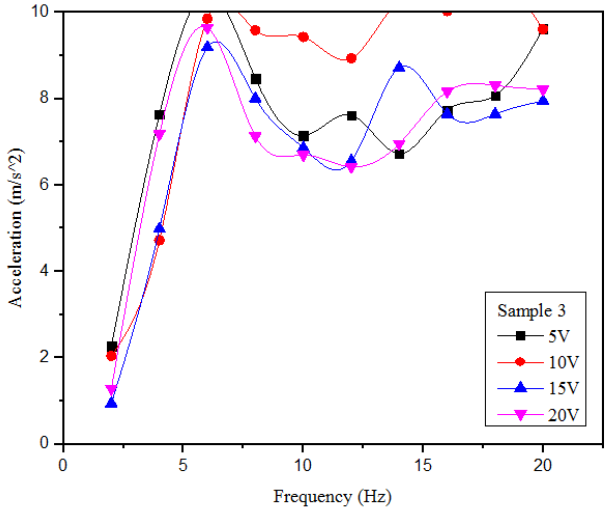

FIG. 64. Acceleration of sample 3

The graph denotes that the acceleration of the vibrating top plate is reduced considerably at different input voltage. The vibrations are arrested at a higher voltage at a high frequency of vibration. The graph denotes that the acceleration of the vibrating top plate is reduced considerably at different input voltage. The vibrations are arrested at a higher voltage at a high frequency of vibration. Due to the resonant conditions of the test apparatus at low frequency the acceleration of the plate is high. The steady output of damping of the vibration is achieved at 10 V for Sample 2.

The displacement values for the 5 V input were obtained for the samples and were tabulated, Table. 11 along with base readings to plot the graph, Fig. 65 of the output performance of the displacement of the piston for each sample which denotes the travel of the damper.

Table 11. Displacement for 5 V (mm)

Frequency (Hz)	Base	Sample 1	Sample 2	Sample 3
2	3.029	4.736	3.057	4.136
4	20.6	20.08	4.032	7.577
6	7.229	7.19	3.011	4.083
8	2.259	1.663	2.014	0.01227
10	0.975	0.895	1.24	0.675
12	0.423	0.514	0.535	0.353
14	0.422	0.398	0.475	0.301
16	0.329	0.344	0.367	0.26
18	0.436	0.192	0.177	0.266
20	0.32	0.165	0.224	0.186

The graph was plotted with tabulated values of displacement for 5 V for each sample taking the applied frequency on the X-axis and the acceleration values on the Y-axis denoting the vibrating acceleration of the top plate concerning the applied voltage. The graph denotes that the displacement of the vibrating top plate is reduced considerably for all the samples. The reduced damper travel or displacement of the top plate denotes that the vibrations are absorbed. The range of the difference in the acceleration of the vibrating top plate is 4.7% to 80% concerning the base readings obtained.

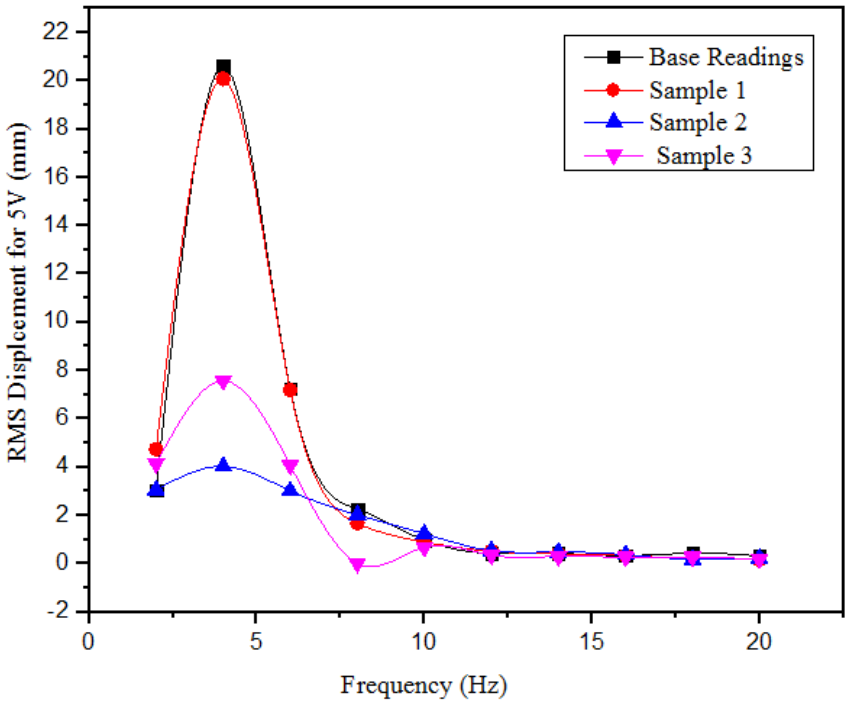

FIG. 65. Displacement for 5 V (mm)

The highest vibration damping for the 5 V input voltage is obtained with sample 2. The steady output for arresting the vibration of the top plate for the entire frequency range is achieved in sample 2 for 5 V input voltage.

The displacement values for the 10 V input were obtained for the samples and were tabulated, Table. 12 along with base readings to plot the graph, Fig. 66 of the output performance of the displacement of the piston for each sample which denotes the travel of the damper. The graph was plotted with tabulated values of displacement for 10 V for each sample taking the applied frequency on the X-axis and the acceleration values on the Y-axis denoting the vibrating acceleration of the top plate concerning the applied voltage. The graph denotes that the displacement of the vibrating top plate is reduced considerably for all the samples.

Table 12. Displacement for 10 V (mm)

Frequency (Hz)	Base	Sample 1	Sample 2	Sample 3
2	3.029	3.267	2.715	3.883
4	20.6	3.27	5.768	4.889
6	7.229	3.262	3.496	4.775
8	2.259	2.136	1.503	1.395
10	0.975	1.242	0.833	0.999

12	0.423	0.668	0.449	0.591
14	0.422	0.583	0.4	0.376
16	0.329	0.626	0.419	0.308
18	0.436	0.228	0.333	0.279
20	0.32	0.204	0.154	0.174

The reduced damper travel or displacement of the top plate denotes that the vibrations are absorbed. The graph was plotted with tabulated values of displacement for 15 V for each sample taking the applied frequency on the X-axis and the acceleration values on the Y-axis denoting the vibrating acceleration of the top plate concerning the applied voltage.

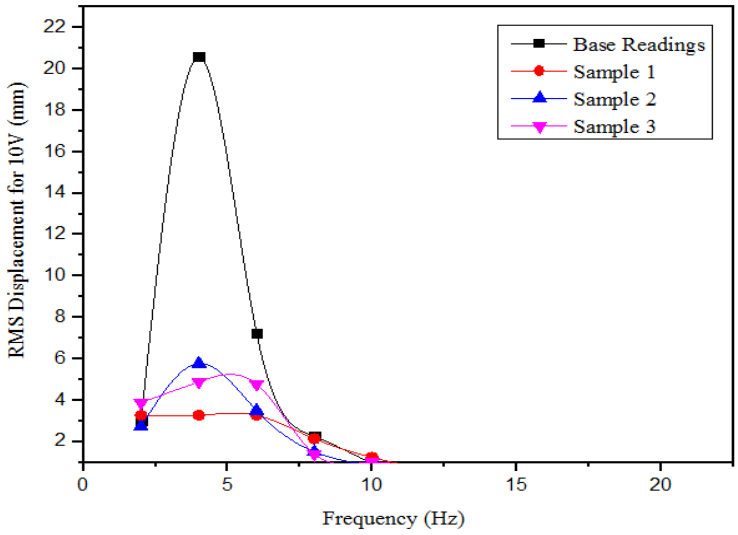

FIG. 66. Displacement for 10 V

The displacement values for the 15 V input were obtained for the samples and were tabulated, Table. 13 along with base readings to plot the graph, Fig. 67 of the output performance of the displacement of the piston for each sample which denotes the travel of the damper. of the damper. The graph denotes that the displacement of the vibrating top plate is reduced considerably for all the samples. The reduced damper travel or displacement of the top plate denotes that the vibrations are absorbed.

Table 13. Displacement for 15 V (mm)

Frequency (Hz)	Base	Sample 1	Sample 2	Sample 3
2	3.029	4.591	2.546	2.731
4	20.6	20.52	8.598	4.698
6	7.229	3.178	6.182	3.6
8	2.259	1.517	1.518	1.512

10	0.975	0.825	0.975	0.685
12	0.423	0.653	0.63	0.419
14	0.422	0.525	0.473	0.357
16	0.329	0.586	0.443	0.262
18	0.436	0.582	0.303	0.262
20	0.32	0.353	0.233	0.185

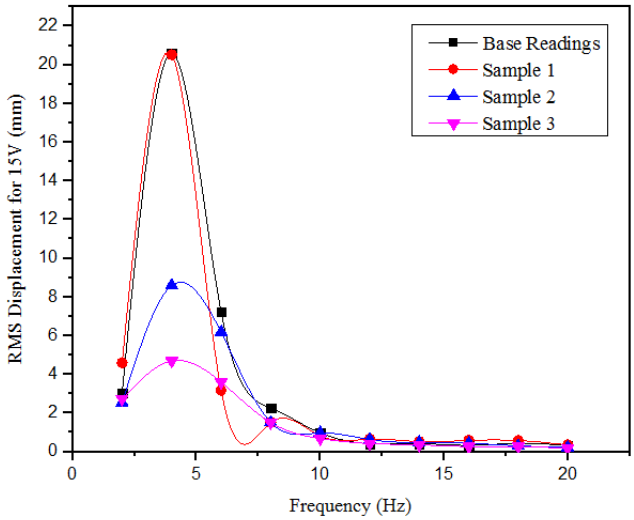

FIG. 67. Displacement for 15 V

The graph denotes that the displacement of the vibrating top plate is reduced considerably for all the samples. The reduced damper travel or displacement of the top plate denotes that the vibrations are absorbed. The range of the difference in the acceleration of the vibrating top plate is 0.1 % to 76 % concerning the base readings obtained. The highest vibration damping for the 15 V input voltage is obtained with sample 3. The steady output for arresting the vibration of the top plate for the entire frequency range is achieved in sample 3 for 15 V input voltage.

Table 14. Displacement for 20 V (mm)

Frequency (Hz)	Base	Sample 1	Sample 2	Sample 3
2	3.029	3.181	4.113	3.087
4	20.6	19.59	9.232	5.769
6	7.229	4.056	2.486	3.951
8	2.259	1.115	1.496	1.095
10	0.975	0.939	0.961	0.638
12	0.423	0.609	0.631	0.464

14	0.422	0.202	0.521	0.321
16	0.329	0.23	0.478	0.32
18	0.436	0.254	0.478	0.233
20	0.32	0.232	0.235	0.191

The displacement values for the 20 V input were obtained for the samples and were tabulated, Table. 14 along with base readings to plot the graph, Fig. 68 of the output performance of the displacement of the piston for each sample which denotes the travel of the damper. of the damper. The graph was plotted with tabulated values of displacement for 20 V for each sample taking the applied frequency on the X-axis and the acceleration values on the Y-axis denoting the vibrating acceleration of the top plate concerning the applied voltage. The graph denotes that the displacement of the vibrating top plate is reduced considerably for all the samples. The reduced damper travel or displacement of the top plate denotes that the vibrations are absorbed. The range of the difference in the acceleration of the vibrating top plate is 4.76% to 76.1% concerning the base readings obtained. The highest vibration damping for the 20 V input voltage is obtained with sample 3. The steady output for arresting the vibration of the top plate for the entire frequency range is achieved in sample 3 for 20 V input voltage.

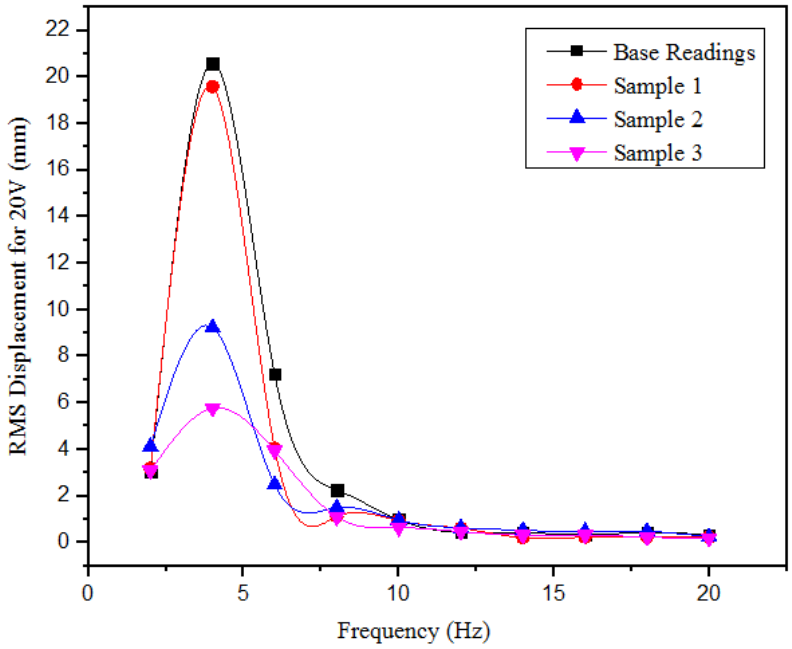

FIG. 68. Displacement for 20 V (mm)

The displacement values for sample 1 were obtained by varying the input voltage and frequency for which the values were tabulated, Table. 15 along with base readings to plot the graph, Fig. 69 of the output performance of acceleration. The graph was plotted with tabulated values of displacement for sample 1 taking the applied frequency on the X-axis and the acceleration values on the Y-axis denoting the vibrating acceleration of the top plate concerning the applied voltage.

Table 15. Displacement of sample 1 (mm)

Frequency (Hz)	5 V	10 V	15 V	20 V
2	4.736	3.267	4.591	3.181
4	20.08	3.265	20.52	19.59
6	7.19	3.262	3.178	4.056
8	1.663	2.136	1.517	1.115
10	0.895	1.242	0.825	0.939
12	0.514	0.668	0.653	0.609
14	0.398	0.583	0.525	0.202
16	0.344	0.626	0.586	0.23
18	0.192	0.228	0.582	0.254
20	0.165	0.204	0.353	0.232

The graph denotes that the displacement of the vibrating top plate is reduced considerably at different input voltage. The vibrations are arrested at a higher voltage at a high frequency of excitation. Due to the resonant conditions of the test apparatus at low frequency, the acceleration of the plate is high at lower frequencies.

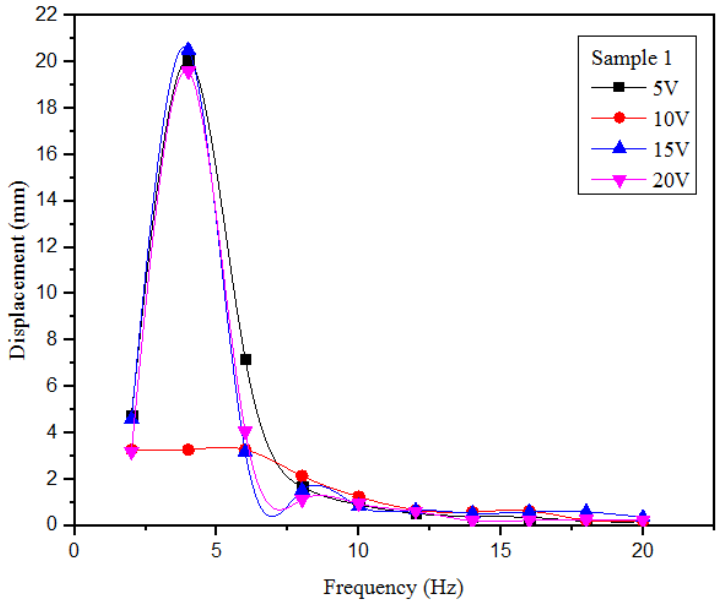

FIG. 69. Displacement of sample 1

The steady output of damping of the vibration is achieved at 10 V for Sample 1. The displacement values for sample 2 were obtained by varying the input voltage and frequency for which the values were tabulated, Table. 16 along with base readings to plot the graph, Fig. 70 of the output performance of

acceleration. The graph was plotted with tabulated values of displacement for sample 2 taking the applied frequency on the X-axis and the acceleration values on the Y-axis denoting the vibrating acceleration of the top plate concerning the applied voltage. The graph denotes that the displacement of the vibrating top plate is reduced considerably at different input voltage. The vibrations are arrested at a higher voltage at a high frequency of vibration.

Table 16. Displacement of sample 2 (mm)

Frequency (Hz)	5 V	10 V	15 V	20 V
2	3.057	2.715	2.546	4.113
4	4.032	5.768	8.598	9.232
6	3.011	3.496	6.182	2.486
8	2.014	1.503	1.518	1.496
10	1.24	0.833	0.975	0.961
12	0.535	0.449	0.63	0.631
14	0.475	0.4	0.473	0.521
16	0.367	0.419	0.443	0.478
18	0.177	0.333	0.303	0.478
20	0.224	0.154	0.233	0.235

Due to the resonant conditions of the test apparatus at low frequency, the acceleration of the plate is high at lower frequencies. The steady output of damping of the vibration is achieved at 5 V for Sample 2.

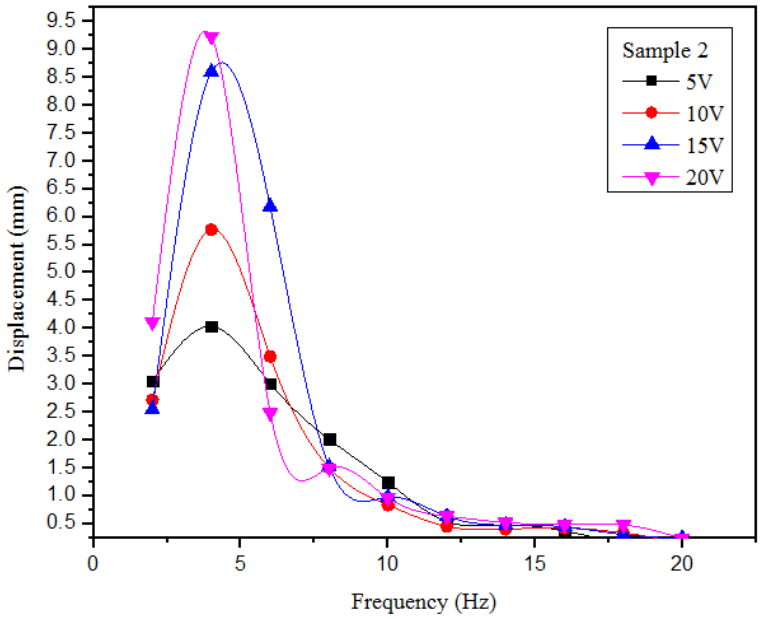

FIG. 70. Displacement of sample 2

The displacement values for sample 3 were obtained by varying the input voltage and frequency for which the values were tabulated, Table. 17 along with base readings to plot the graph, Fig. 71 of the output performance of acceleration. The graph was plotted with tabulated values of displacement for sample 3 taking the applied frequency on the X-axis and the acceleration values on the Y-axis denoting the vibrating acceleration of the top plate concerning the applied voltage.

Table 17. Displacement of sample 3 (mm)

Frequency (Hz)	5 V	10 V	15 V	20 V
2	3.057	2.715	2.546	4.113
4	4.032	5.768	8.598	9.232
6	3.011	3.496	6.182	2.486
8	2.014	1.503	1.518	1.496
10	1.24	0.833	0.975	0.961
12	0.535	0.449	0.63	0.631
14	0.475	0.4	0.473	0.521
16	0.367	0.419	0.443	0.478
18	0.177	0.333	0.303	0.478
20	0.224	0.154	0.233	0.235

The graph denotes that the displacement of the vibrating top plate is reduced considerably at different input voltage. The vibrations are arrested at a higher voltage at a high frequency of vibration.

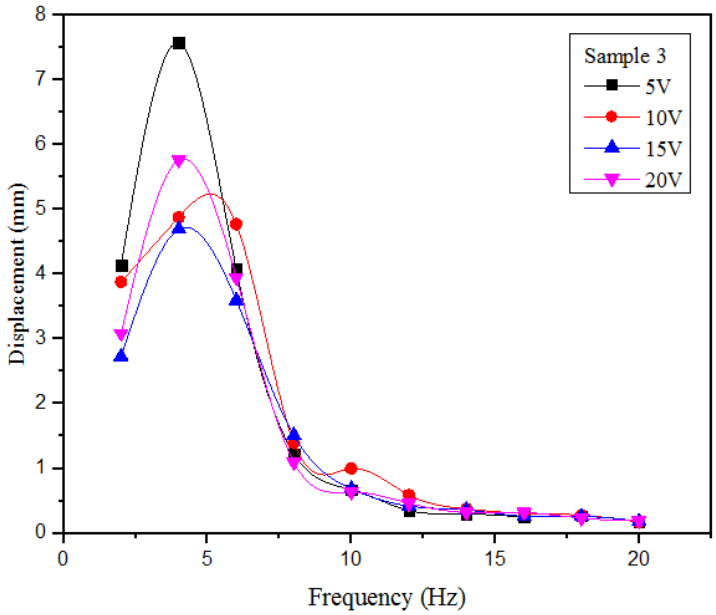

FIG. 71. Displacement of sample 3

Due to the resonant conditions of the test apparatus at low frequency, the acceleration of the plate is high at lower frequencies. The steady output of damping of the vibration is achieved at 15 V for Sample 3.Thus, the fluids respond to the magnetic field and arrest the vibration-reducing the displacement of the top plate. The performance is better with thick fluid for higher vibration frequencies.

2.12. Theoretical analysis

The theoretical analysis of the output performance is analyzed using MATLAB. The following steps are carried out to create the MATLAB Simulink model of the semi-active suspension which was tested experimentally on the quarter car model. The model is created by converting the free body diagram of a quarter car model setup with semi-active or magnetorheological fluid suspension and reducing their equations of motion to determine the governing factors K/m and C/m values.

1. The MATLAB Software is opened, and the Simulink library is accessed to obtain the commonly used blocks.
2. The Integration /Gain and Sum operators are added using the commonly used blocks dialogue box.
3. The Simulink Library is opened, and the Source is selected to add the sinewave operator to the model.

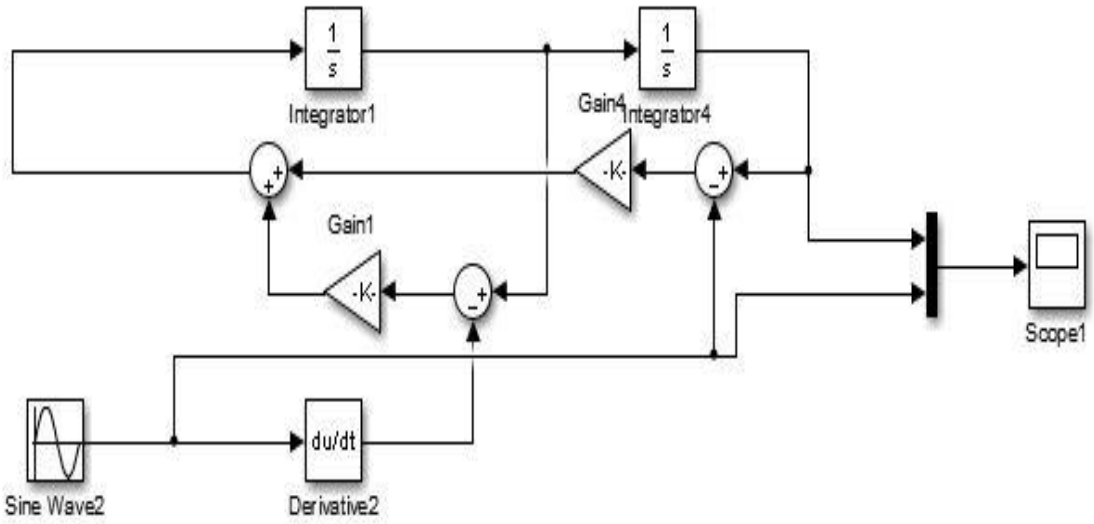

FIG. 72. Simulink model

4. Then, the Simulink Library is opened, and the Sinks option is selected, and the Scope operator is added to the model.
5. The operators are placed in the required positions and are connected using connecting lines to the multiplexer to the scope.
6. The values of k/m and c/m are given to the gain as input data for the Simulink model as shown in Fig. 72 and 74
7. The scope is selected; the play option is selected to run the entered data to obtain the signal waveform for the corresponding values.

8. The scope is selected, and the generated waveform is displayed.
9. The procedure is repeated to create similar Simulink models for the input of three different samples to generate the combined wave in Fig. 73.

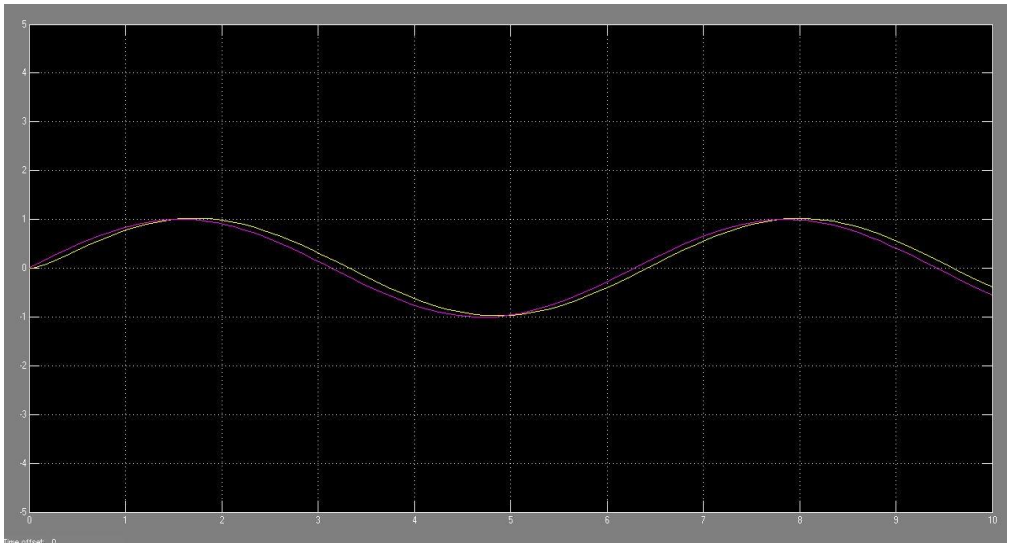

FIG. 73. Generated wave form

10. The calculated values of K/m and C/m are entered, and the wave is generated for 5 V, 10 V, 15 V & 20 V respectively.

Table 18. Values of (C/m)

Input voltage	Sample 1	Sample 2	Sample 3
5 V	8	4.4	3.6
10 V	6.2	3	5.6
15 V	3.8	3.4	3.4
20 V	4	3.6	3.8

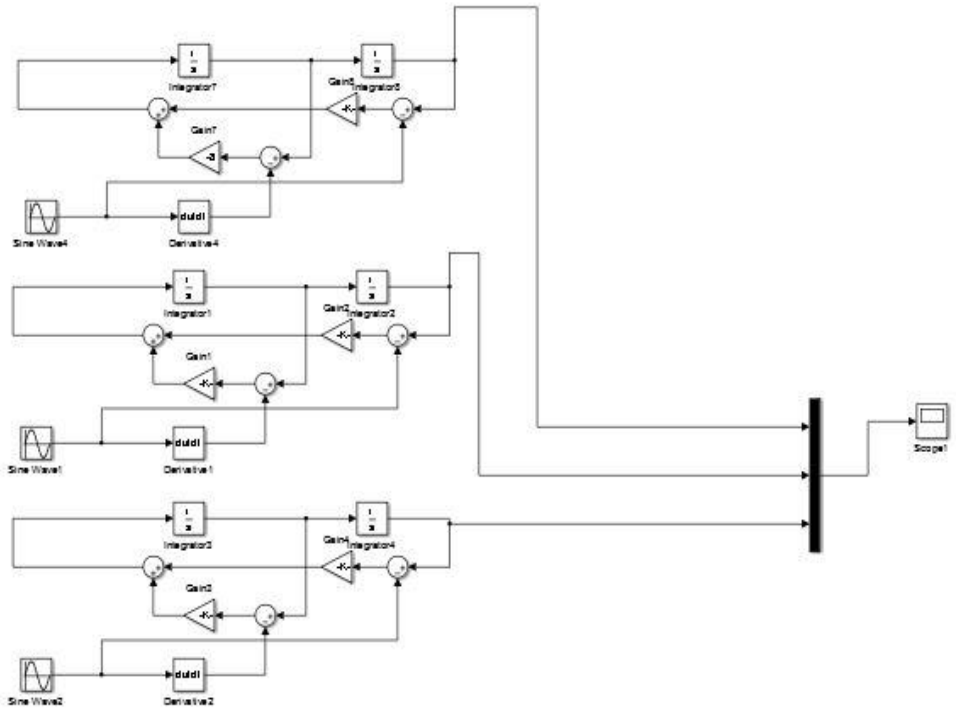

FIG. 74. Combined simulink model

The combined output waveform generated for the 5 V input voltage in Fig. 75 where Yellow denotes Sample 1, Pink denotes Sample 2, and Blue denotes Sample 3.

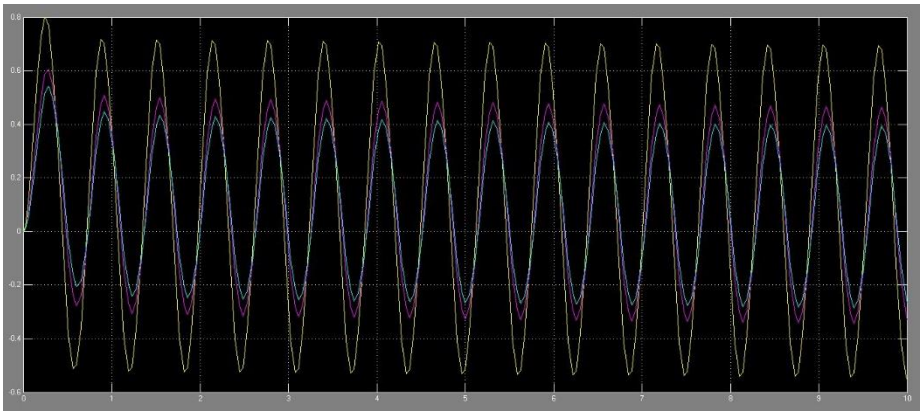

FIG. 75. 5 V wave form

The combined output waveform generated for the 10 V input voltage in Fig. 76 where Yellow denotes Sample 1, Pink denotes Sample 2, and Blue denotes Sample 3.

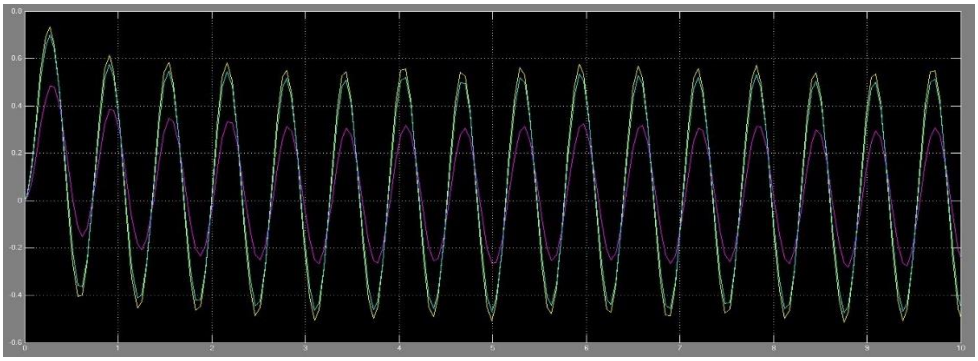

FIG. 76. 10 V wave form

The combined output waveform generated for the 15 V input voltage in Fig. 77 where Yellow denotes Sample 1, Pink denotes Sample 2, and Blue denotes Sample 3.

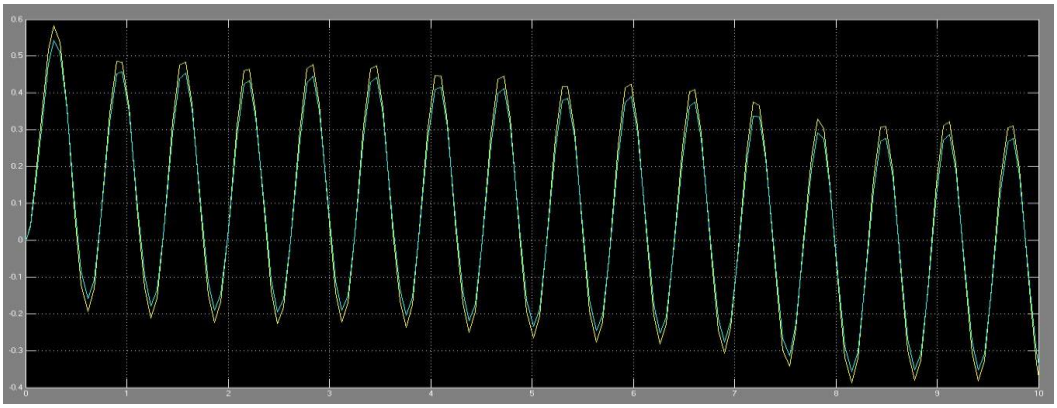

FIG. 77. 15 V wave form

The combined output waveform generated for the 20 V input voltage in Fig. 78 where Yellow denotes Sample 1, Pink denotes Sample 2, and Blue denotes Sample 3.

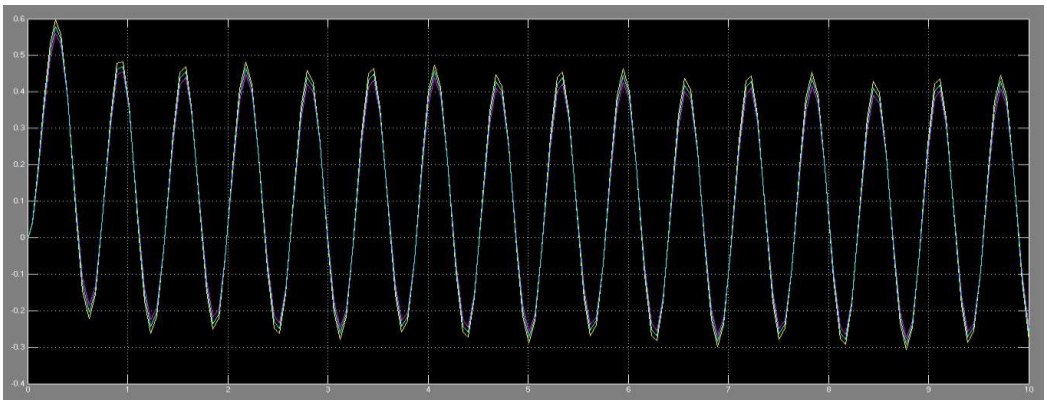

FIG. 78. 20 V wave form

The theoretical waveforms were arrived with a similar pattern to that of the experimental by the Simulink model.

3. Business Analytics

3.1. Facility Layout Plan

The basic classification of the layouts in production based on the size of the industry and pattern of the production follow carried out is discussed to categorize the large variety. The key focus of the research was to establish the easiest way to develop an effective and maintenance-free layout with minimal effort by classifying certain parameters [31]. With this research as a reference, a simple layout was built on a small-scale industry basis. The intricacy of the designed layout model can be determined by using some simple denotations and parameters to analyze the layout. These are discussed and elaborated by researchers to understand the link between the factors or parameters that govern the complexity of the layout structure. [32].

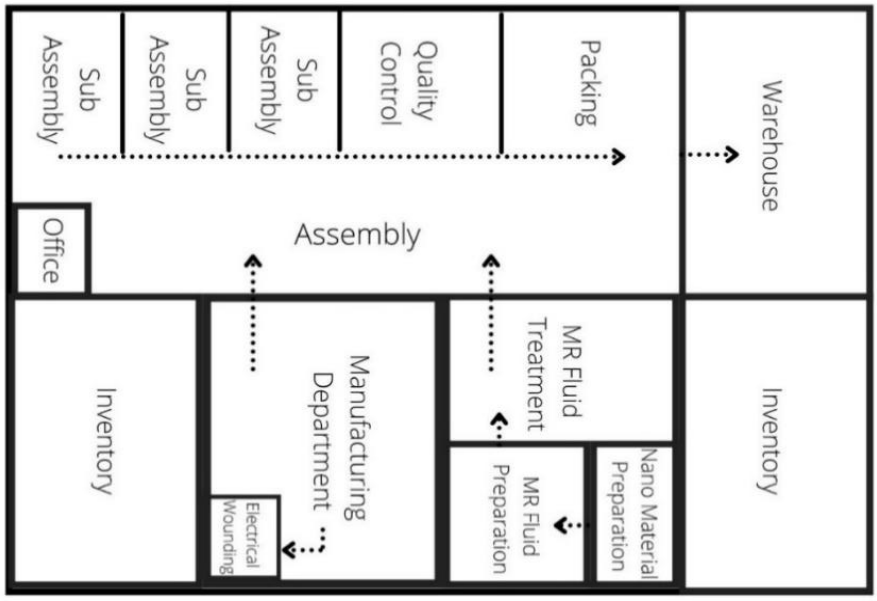

FIG. 79. Factory layout

The potential geographical and market conditions were analyzed to determine the challenges in starting up a new manufacturing industry to manufacture the designed damper. The market analysis was done to determine the potential competitors, their features, and sales background to obtain data on their product and customer requirements. The product is altered and tailored to fit customers of different transport users. The layout of the manufacturing unit was designed in a way that movement between departments is reduced as much as possible by keeping the process cycle a guideline to avoid rerouting. The manufacturing line is separated into three different departments with multiple stages of the process namely: fluid preparation department, manufacturing department, and assembly department respectively, and the process flow chart in Fig. 79 and 80.

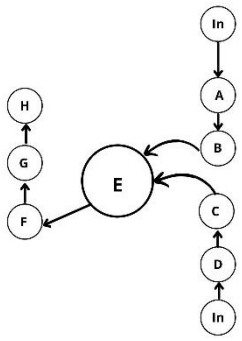

FIG. 80. Process flowchart

The plant layout is converted into a progression flow chart to ease the process of evaluating the intricacy of the layout by certain parameters called density index and path index as explained and indicated by previous researches.[8] The density index is the measure of the ratio of several graph nodes to the theoretical maximum number of those nodes connecting all the nodes, where k is the actual number of connections and n is the number of nodes as shown in equation (1). The density index for the designed layout is 0.16. The path index denotes the ideal deviation in the theoretical and practical number of paths in the layout as shown in equation (2). The obtained parametric values denote that the designed layout is a simple layout with the sequential process for which cycle index, decision point index, and redundancy distribution index are not necessary to be evaluated.

$$Density\ Index = \frac{k}{n(n-1)} = \frac{9}{8(8-1)} = 0.160 \quad (1)$$

$$Path\ Index = 1 - \frac{p}{N} = 1 - \frac{2}{2} = 0 \quad (2)$$

3.2. Cost Estimation and Break-Even Analysis

There are several techniques based on which the manufacturing costs are estimated using artificial intelligence, enterprise resource planning, and computer-aided designed integrated cost estimation. Researchers have created a paper that deals or guides on how to select a cost estimation technique based on the innovation quotient factor and value of the manufacturing products using a decision tree. This has been formulated using several previous references and works of literature to support and validate different methodologies [33].

The break-even analysis is the method adopted to determine the point or quantity of sales wherein the establishment yields neither a profit nor a loss by breaking even with the costs inquired to develop and establish the industry or business. This is the most used technique to determine the break-even point in a business. The parameters that govern this calculation are the fixed costs, variable costs, and selling price per unit. The fixed costs are otherwise known as the constant expenditure during business such as the rent, salary, equipment, and setup costs. The variable costs are the material costs, electricity, maintenance, and emergency expenditures. These are usually manually calculated to determine the approximate units to formulate business strategies to plan. Researchers have contributed to the digitalization of this calculation to ease the effort. The possibility of artificial intelligence is being exploited to determine the break-even quantity and productivity of a textile industry that deals with more than 1000 variants of fabrics and its products [34].

The break-even point for battery trucks in Latin American states is obtained using a model which involves varying factors that are geographical-based conditions. The obtained results have helped to conclude the trend in each state by considering the current status and predicted future scenarios along with exceptions and advertising [35].

The firm is set to handle a global e-commerce market with a standard retail market price for single unit purchases and customize the product for bulk industrial orders or function as a supplier. The average costs of setting up the manufacturing industry, equipment, labor, material, electricity, advertising, and packaging charges were estimated. These estimated values are as tabulated in Table.s 19 and 20. These numbers were used to calculate the break-even unit of the damper with a standard retail selling price of 600 €. The labor rates in Lithuania were defined as 8.8 € per hour in the Eurostat released in April 2019. [38,39] This figures was used to determine the approximate labor charges enquired depending on the planned schedule of work. The average rent rate in Lithuania was stated to be 3-5 € per m^2. [38,39] The plant layout was estimated to be established for approximately 3000 m^2. The approximate price of the equipment and charges were estimated to contribute to the equipment and setup charges. The variable cost of the product is assumed to be 100 €. The break-even point of the sales as the number of units was calculated using the formula below. The estimated total fixed cost is approximately 317000 €.

Table 19. Estimated fixed costs (€)

Fixed Costs (€)	
Rent	180000
Salary	19008
Equipment	115464.6
Setup	1760
Total	316323.6

$$Break\ even\ unit = \frac{FC}{SP - VC} \quad (3)$$

Where, *FC* – Fixed Costs; *SP* – Selling price per unit; *VC* – Variable price per unit

These calculations were made with certain detailed planning for the functioning of the industry. The industrial layout was planned for 3000 m^2 area of land with basic construction building and internal detailing. The break-even point was calculated to be 634 units using equation (3). The break-even graph in Fig. 81.

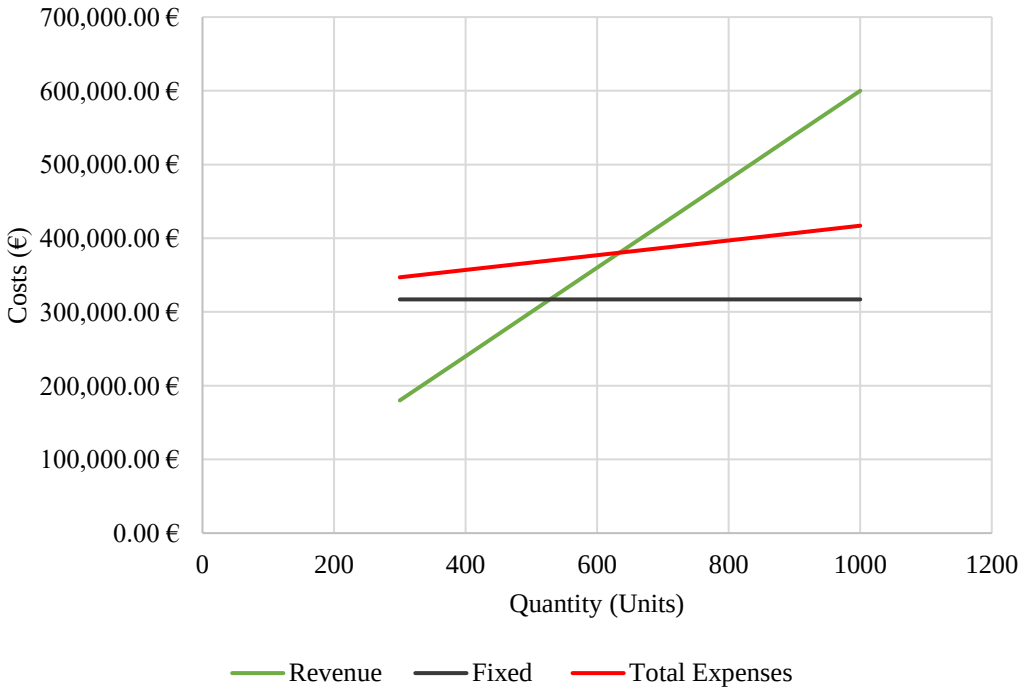

FIG. 81. Break-even analysis

The graph indicates the slow growth of revenue with a surge in sales to achieve a breaking point with the total expenses. Similar calculations were performed for different variable costs per unit of the damper to obtain a view of the units to be sold to break even. The obtained values are tabulated in Table. 20 and a graphical representation of the comparison of variable cost per unit that can affect the break-even point in the graph in Fig. 82.

Table 20. Break-even units for different variable costs per unit (€)

Scenario	BE in units	Variable cost per unit (€)
Case 1	576.3	50
Case 2	634	100
Case 3	704.4	150
Case 4	792.5	200

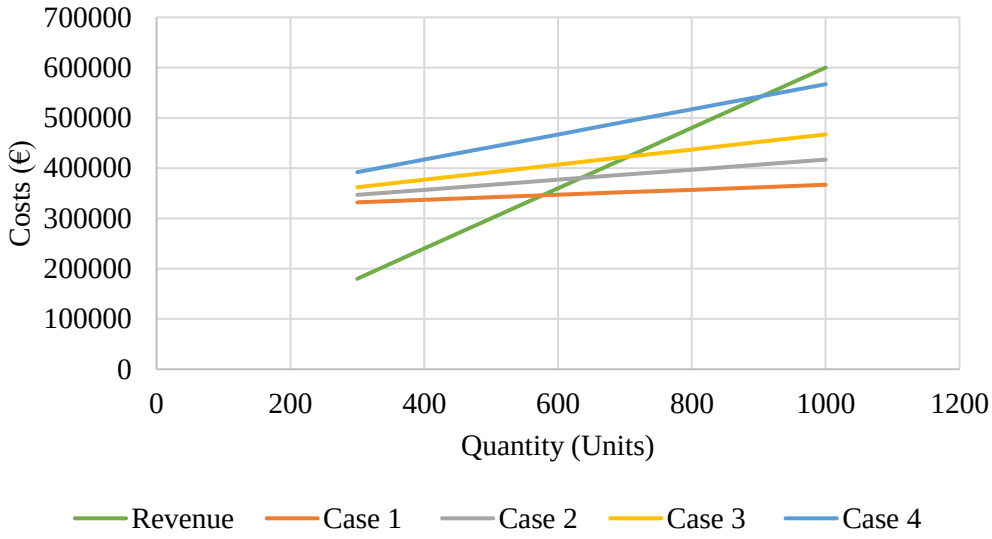

FIG. 82. BEP for different variable costs per unit (€)

3.3. Sales Prediction using Bass Diffusion Model

The basic equation is used to analyze considered the values of the coefficient representing the different sales scenarios. Several researchers have adopted this model to obtain forecasts of the outcome assuming different scenarios and how it could affect the market trend.[36] The method of analyzing the sales data history of similar technology in the market for its market trend has been adopted generally in several research papers with uncertainty factors. The Bass diffusion model is employed as a robust model with the available historic data to adapt to the new technology. In research, to launch a new call model which was similar to an existing model in the market was analyzed using the bass diffusion model to obtain the sales forecast outcomes.[37] Based on the diffusion of innovations theory, the Bass diffusion model predicts the number of adopters of an invention or device using different parameters such as relative benefit, observability, reinvent ability, trialability, compatibility, and difficulty. The innovators and imitators, which are the two consolidated parameters of the discussed variables, are used to decide the adopters. The innovators are a group of people who adapt to a new product without waiting for a review or input from existing customers, whereas the imitators are a group of people who are influenced by previous adopters. The formula below can be used to generate the rate of acceptance and the quantity of adaptors at the nth year as shown in equation (4).

$$n(t) = p * [m - N(t)] + \left(\frac{q * N(t)}{m}\right) * [m - N(t)] \quad (4)$$

Where *n(*t*)* is the number of adopters at time t with a market potential of m; *N(*t*)* cumulative adopters at time *t*; *p* is the coefficient of adoption of innovators and *q* is the coefficient of adoption of imitators. With this equation, the model prediction can be made using different values of *p* and *q* where it can be stated that $0 \geq p,q \geq 1$. For a business model analysis, *p* ranges from 0 - 0.03 and *q* ranges from 0.3 - 0.5 of which 0.38 is said to be an idealistic value. For this purpose of study three different values of each set is of *p* and *q* is considered as a case and the prediction for the sales outcomes are calculated to analyze the market trend in Table. 21.

Table 21. Parameter description of futuristic scenarios

Description	Assumed Scenarios	*p* Value	*q* Value
Case 1	Steady advertising and marketing of the damper and it‘s features	0.01	0.34
Case 2		0.02	0.34
Case 3		0.03	0.34
Case 4	Steady advertising and marketing of the damper and it‘s features with additional discounts	0.01	0.36
Case 5		0.02	0.36
Case 6		0.03	0.36
Case 7	Accelerated advertising and marketing of the damper with added feature to enhance safety	0.01	0.38
Case 8		0.02	0.38
Case 9		0.03	0.38

For the above-mentioned set of parameters, the base model was used to estimate the damper's expected sales quantity in Lithuania. Despite external factors such as accelerating population growth and leading to improved vehicle demand for comfort and efficiency, the forecasted sales Fig.ures reflect the acceptance of the MR dampers by the consumer potential.

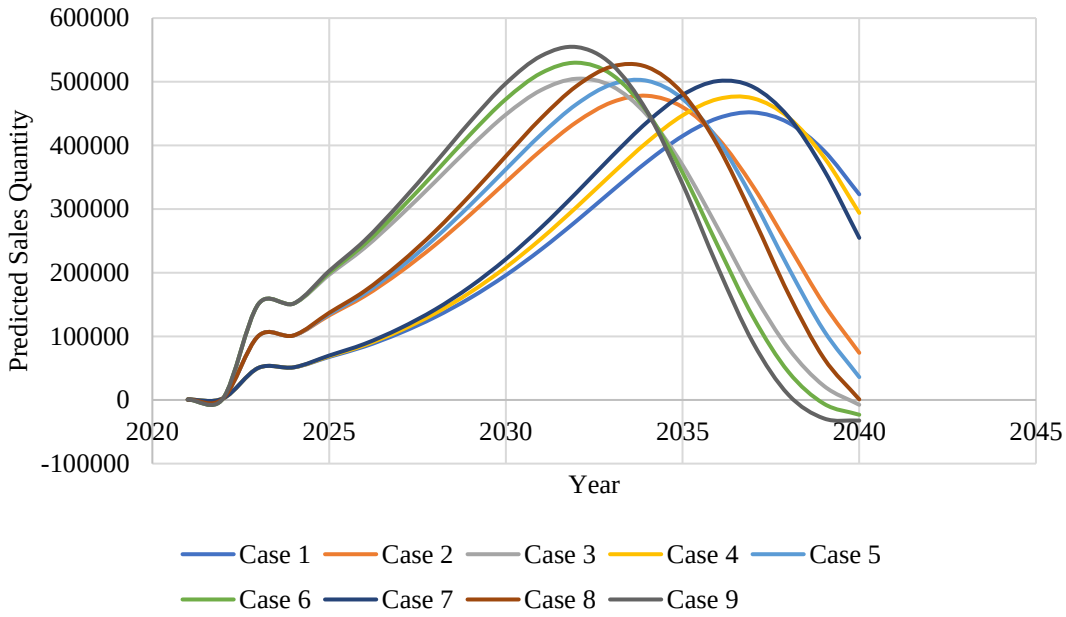

FIG. 83. Predicted sales

The obtained forecasted revenue volumes were plotted on a Table., along with the demand growth for each year. The bass model was used on the MR damper for the nine cases in this analysis, as seen in Table. 21. To assess the pattern of influence of the diffusion parameter values, the different forecast revenue figures were plotted against the year as a graph. From all the obtained graphs it is evident that

the parameters affect the capture of the market and the peak sales duration varies with the parameter and initial sales values. The forecasted sales quantity graph in Fig. 83.

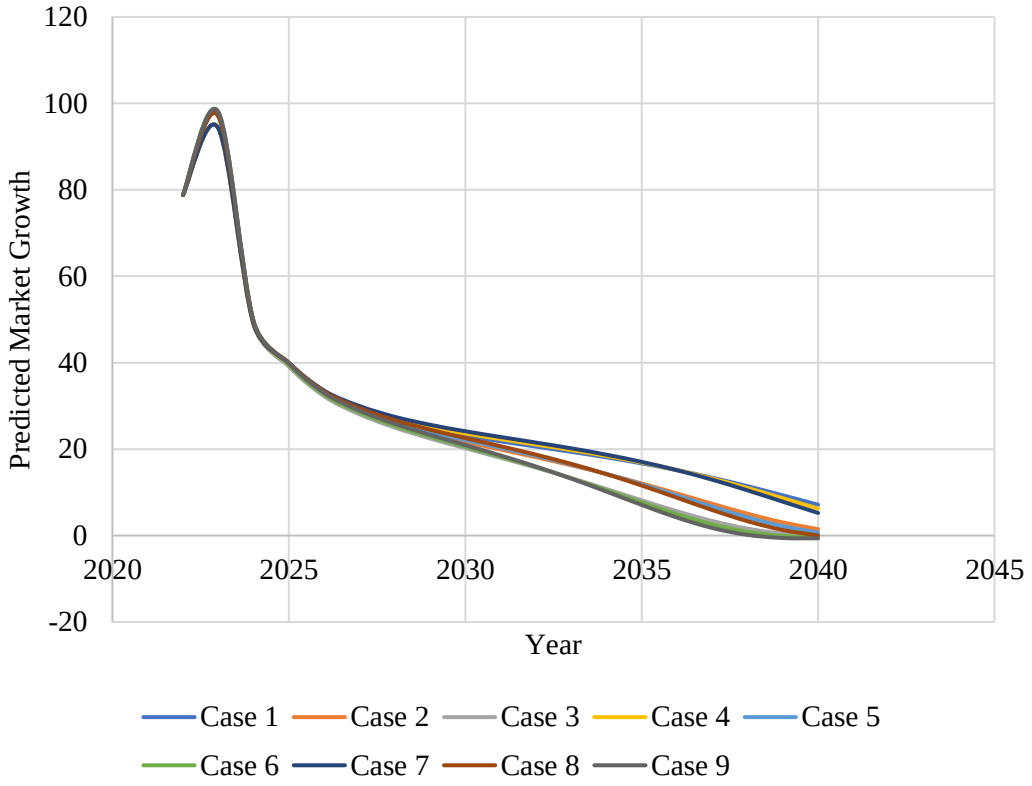

FIG. 84. Predicted market growth

The predicted market growth is indicated in Fig. 84. The sales quantity curve depends on the *p* and *q* parameters and the consequence of the parameters can be seen in the graph, the graph tends to have an early peak point when the *q* values are greater and tend to have a quicker sales fall. From the graph and trend in Lithuania concerning the sales observed, we can conclude that the most ideal values of the parameter are cases 1 and 2 for a steady business.

4. Discussion, Challenges, and Future Scope

The research holds a huge scope for further development in different aspects as this study was mainly intended at assessing the new fluid composition and response. The damper model can be modified by using alloy to relatively decrease the weight, stroke length can be increased to produce better damping results for a luxurious ride, the study can be conducted on a twin-tube MRF damper and bore diameter can be increased to withstand high temperatures. The coil windings employed in this research can be replaced by thicker wires for high range magnetization. A self-altering voltage or coil method can be considered while designing the damper prototype. The comparative study of polydispersed magnetic particles and nanomagnetic particles can be conducted to estimate the effect of size and arrangement of particles in the MR fluid damper. There still exists a scope to improve the steadiness of the fluid by determining the effect of different surfactants for varied applications to achieve the appropriate performance output.

The break-even analysis briefly indicates the year in which the break-even quantity will be achieved. The various cases and their outcomes are also indicated to avoid unexpected outcomes in the case of uncertainty. With these ahead calculations we can evaluate the sales and respective profits obtained. The change in selling price and contribution margin and greatly affect the duration at which the break-even point will be achieved. We can change the parameters dependently to alter the outcomes according to need. The ideal sales trend with an expected rate of 10% of the break-even quantity achieved is furnished from the study. The trend clearly explains how the bass model constraints affect the sales trend. The company can take necessary actions to accelerate the sales using different business strategies such as advertising, marketing through discounts and replacement offers. These show that there is an existing potential market to achieve and conquer. These discussed Figures approximate the methodology to estimate similar business establishments. This research focuses on how a new product can be potentially integrated into the new mobility launch in the country to impact the market to accelerate the market capture by eventually showing the difference in the quality of the product compared to the existing ones in the market. This research is to determine the break-even time and sales trend to obtain declension and peak periods to essentially plan business plans to alter the sales as required.

Certain threats must be given attention to before establishment. The existence of secondary automobile and parts market will deviate the potential customers due to the lack of information or knowledge on the new product and its efficiency. The purchasing capacity of the population of the country will affect the expected sales outcomes [46]. The vending price of the new product may not be adhering to customers due to a variety of alternative options. Strategic business planning along with research and development of the product can alter potential threats. With these strategies combined along with the strategic planning of the launch and development of autonomous vehicles employing this damper as a ride comfort feature in Lithuania can greatly affect the efficiency and quality of the vehicles indeed increasing the factor of imitators in the Bass diffusion model contributing to improved market capture. The introduction of this MR damper into the market as a feature of the autonomous vehicles can prove to be a game-changing factor that elevates the establishment of the product and brand to obtain new retail and commercial customers which will be beneficial to build the business to slowly become a leading damper manufacturing industry globally. Further research can be executed in the technical aspects of this damper

and its integration into the autonomous vehicle. The data integration of the road conditions from various sensors such as the LIDAR and image sensing camera should be converted and given as data input to the variable damping altering unit in the damper system to continuously update the damping effects depending on the load conditions at that instant. This research scope can reform certain aspects of the performance of vehicles considering the data transfer system on connected vehicle systems in the European Union (EU). The instant information exchange on the status of road conditions and vehicles in certain lanes can be utilized to instantaneously adapt vehicle systems or in this case, suspension systems to perform with the expected outcome considering the equipped scope of future vehicles and autonomous vehicles.

Conclusion

There are several conclusions that can be arrived from the research which are as follows,

1. The composition of the MR fluid was altered taking into consideration of all the discussed potential challenges from the literature to overcome certain aspects of downside faced with employing conventional MR fluids. The oxidation of particles will not occur in the proposed composition as there is no valency in the nickel atoms. The presence of both micro and nano particles in the fluid will increase the stability of the fluid.
2. The nano material and nano fluid characteristics were evaluated by SEM and rheometer testing. From the SEM results, the coexsistence of micro and nano particles is evident. The rheometer graphs prove that the fluid is a non newtonian fluid with varying properties at different conditions.
3. A scaled prototype of the damper was manufactured to suit installation scope given in the quarter car model for experimental testing according to the state dimension in the methodology section.
4. The damping charateristics of the sample at various conditions were experimentally tested to have a maximum efficiency of 91.66 % of arresting the base vibrations. When an input voltage of 5 V was given sample 2 proved to be efficient composition with a damping capacity 4.7 % - 80 % of the excitation frequency. Similarly, for 10 V input voltage was given sample 2 proved to be efficient composition with a damping capacity 3.2 % - 89.3 % of the excitation frequency. Similarly, for 15 V input voltage was given sample 2 proved to be efficient composition with a damping capacity 0.1 % - 76 % of the excitation frequency. Similarly, for 20 V input voltage was given sample 2 proved to be efficient composition with a damping capacity 4.76 % - 76.1 % of the excitation frequency. The testing conducted on the different concentrations of the fluid experimentally proved the efficiency of the concentrated samples at higher input voltages. To conclude, a higher concentration of this MR fluid damper can be utilized for heavy loading conditions whereas the lower concentrations can be used for relatively low frequency loading conditions.
5. The functioning and cost of establishment of a small-scale damper OEM industry based on the facility layout plan was created and summarised to carry out business analytics. The density index was determined to be 0.16 and the path index was 0 which denotes that the density of process flow is simple and there is not intervention of path between two process.
6. The business analytics tools: break-even analysis and bass diffusion model was used to analyse the market trend and business flow to generate a strategic plan according to the predicted outcomes. The break-even analysis estimated the BEP to be 634 units when the variable cost is 100€. From the bass diffusion model, the peak sales can be achieved anywhere between the year 2032-2037 depending on the imitators. This indirectly indicates the market trend and the declension of market growth gradually from the year 2025-2037 below which it will yield a loss, or the product will reach a saturation point for which necessary research and development must strategically made to alter the trend.

References

[1] Wikipedia – Car Suspensions [online] 2020 [Viewed on 1 June 2020] Available From: https://en.wikipedia.org/wiki/Car_suspension#History_2

[2] Mech Tech – Types of Suspension System [online] 2014 [Viewed on 1 June 2020] Available From: http://4mechtech.blogspot.com/2014/09/types-of-suspension-system.html

[3] Monroe – Front Suspensions [online] 2020 [Viewed on 1 June 2020] Available From: https://www.monroe.com.au/trade-corner/tech-info/suspension-systems/front-suspensions.html

[4] AIZUDDIN FAHMI MOHD RIDUAN, NOREFFENDY TAMALDIN, AJAT SUDRAJAT, AND FAUZI AHMAD. Review on Active Suspension System, SHS Web Conference 49, ICES 2018. DOI: 10.1051/shsconf/20184902008

[5] Wikipedia – Magnetorheological Damper[online] 2020 [Viewed on 1 June 2020] Available From: https://en.wikipedia.org/wiki/Magnetorheological_damper

[6] Parker LORD – How does an MR Damper Work? [online] 2020 [viewed on 1 June 2020] Available From: https://www.lord.com/products-and-solutions/active-vibration-control/industrial-suspension-systems/how-does-mr-damper-work

[7] RONGHUI ZHOU, ARGYRIOS ZOLOTAS, ROGER GOODALL. Intergrated Tilt with Active lateral suspension control for high speed railway vehicles, Elsevier – Mechatronics, Volume 21, Issue 6, September 2011. DOI: 10.1016/j.mechatronics.2011.07.001

[8] PAWEL SKALSKI, WERNIKA SLUOWSKA. Review of Magnetorheological Dampers, In: Proceedings of the Institute of Vehicles 3(112)/2017

[9] ABHIJEET N. KULKARNI, SANTOSH R. PATIL. Magneto-Rheological (MR) and Electro-Rheological (ER) Fluid Damper: A Review Parametric Study of Fluid Behavior, In: Journal of Engineering Research And Applications, ISSN: 2248-9622, Vol.3, Nov-Dec 2013, pp. 1879-1882.

[10] NIKHIL DESAI, BHARATBHUSHAN KALE. A Review Work on Suspension Systems Models, Control Strategies for Suspension System, Journal of Emerging Technologies and Innovative Research (JETIR), Volume 3, Issue 10, October 2016.

[11] SA WAHID, I ISMAIL, S AID, MSA RAHIM. Magneto- Rheological Defects and Failures : A Review, IOP Conferences, Materials Science And Engineering 114, 2016 DOI: 10.1088/1757-899X/114/1/012101

[12] G.Z. YAO , F.F. YAP, G. CHEN, W.H. LI, S.H. YEO. MR damper and its application for semi-active control of vehicle suspension system, Elsevier, Pergamon- Mechatronics 12 (2002) 963-973

[13] ZOHIR BENLAHCENE, WALEED F FARIS, MD RAISUDDIN KHAN AND S.I. IHSAN. Semi-Active Suspension System for Off-Road Vehicles, In: Proceedings of the 3rd International Conference on Mechatronics, ICOM'08 18 – 20 December 2008

[14] MOHAMMAD MEFTAHUL FERDAUS, MUHAMMAD MAHBUBUR RASHID, MST. NAFISA TAMANNA SHANTA, MUHAMMAD HASIBUL HASAN. Experimental Investigation on Magnetorheological Damper's characterization, Advanced Materials Research Vol 1115 (2015) pp 476-479, Trans Tech Publications, Switzerland 2015. DOI: doi:10.4028/www.scientific.net/AMR.1115.476

[15] SIDHARTH SHARMA, SUMANYU KHURANA. Investigation on Magnetorheological Damper for Its Various Applications, International Journal of Latest Technology in Engineering, Management & Applied Science (IJLTEMAS) Volume VI, Issue XI, November 2017 | ISSN 2278-2540

[16] BOGDAŃ SAPIŃSKI, MARCINSZCZĘCH. CFD Model Of A Magnetorheological Fluid In Squeeze Mode, Acta Mechanica et Automatica, vol.7 no.3 (2013). DOI: 10.2478/ama-2013-0031

[17] SADAK ALI KHAN, A. SURESH, N. SEETHA RAMAIAH. Principles, Characteristics and Applications of Magneto Rheological Fluid Damper in Flow and Shear Mode. Elsevier - 3rd International Conference on Materials Processing and Characterisation (ICMPC 2014). DOI: 10.1016/j.mspro.2014.07.136

[18] G R PENG, W.H.LI, H.DU, H.X. DENG, G. ALICI. Modelling and Identifying the parameters of a Magnetorheological damper with a force lag phenomenon, Elsevier – Applied Mathematical Modelling 38, 2014. DOI:10.1016/j.apm.2013.12.006

[19] X.C. GUAN, P.F. GUO, J.P. OU. Modeling and Analyzing of Hysteresis Behavior of Magneto Rheological Damper, Elsevier - The Twelfth East Asia-Pacific Conference on Structural Engineering and Construction, Procedia Engineering 14 (2011) 2756–2764 DOI: 10.1016/j.proeng.2011.07.347

[20] T.IMTHIYAZAHAMED,R.SUNDARRAJAN,G.T.PRASAATH,V.RAVIAJ. Implementation of Magneto-rheological dampers in bumpers of Automobiles for reducing impacts during accidents, Elsevier - 12th Global Congress On Manufacturing And Management, GCMM 2014, Procedia Engineering 97 (2014) 1220 – 1226 DOI: 10.1016/j.proeng.2014.12.400

[21] R N PATIL SAGAR RAJENDRA, WALUNJ PRASHANT YERRAWAR, DR.R.R.ARAKERIMATH, SAMBHAJI. International Journal of Innovative Research in Science, Engineering and Technology, Vol. 3, Issue 12, December 2014. DOI: 10.15680/IJIRSET.2014.0312075

[22] I. MIHAI, F. ANDRONIC. Behavior of a semi-active suspension system versus a passive suspension system on an uneven road surface, ISSN 1392 - 1207. MECHANIKA. 2014 Volume 20(1): 64-69 DOI: 10.5755/j01.mech.20.1.6591

[23] Nickel Iron Oxide / Nickel Ferrite (NiFe2O4)Nanoparticles - Properties, Applications, In: US Research Nanomaterials, Inc., July 2013.

[24] JOSEPH SCOTT BUNCH. Mechanical And Electrical Properties Of Graphene Sheets, Presented to the Faculty of the Graduate School of Cornell University.

[25] NALINA. H.V, ANDRIUS. D. Research on Semi Active Suspensions in Passenger Car. Proceedings od 24th International Scientific Conference. Transport Means, 1010-1016. 2020.

[26] PRASAD. N. H, RAJYALAKSHMI. G, REDDY. A. S. A typical manufacturing plant layout design using CRAFT algorithm. *Procedia engineering*, *97*, 1808-1814. 2014.

[27] POURVAZIRI. H, PIERREVAL.H, MARIAN. H. Integrating facility layout design and aisle structure in manufacturing systems: Formulation and exact solution. *European Journal of Operational Research*, *290*(2), 499-513. 2021.

[28] TAYAL. A, SOLANKI. A, SINGH. S. P. Integrated framework for identifying sustainable manufacturing layouts based on big data, machine learning, meta-heuristic and data envelopment analysis. *Sustainable Cities and Society*, *62*, 102383. 2020.

[29] AL-ZUBAIDI. S. Q. D, FANTONI. G, FAILLI. F. Analysis of Drivers for Solving Facility Layout Problems: Literature Review. *Journal of Industrial Information Integration*, 100187. 2020.

[30] GAMBERINI. R, RUGGERINI. T, LOLLI. F. The plant layout of a foundry: Constraints, operative guidelines and a case study. *IFAC-PapersOnLine*, *51*(11), 1180-1185. 2018.

[31] GAYAM. N. R, SHANMUGANANDAM. K, VINODH. D. Layouts in production industries: A review. *Materials Today: Proceedings*. 2020

[32] ELMARAGHY. H, ALGEDDAWY. T, SAMY. S. N, ESPINOZA. V. A model for assessing the layout structural complexity of manufacturing systems. *Journal of Manufacturing Systems*, *33*(1), 51-64. 2014.

[33] SCHWABE. O, SHEHAB. E, ERKOYUNCU. J. An approach for selecting cost estimation techniques for innovative high value manufacturing products. *Procedia CIRP*, *55*, 41-46. 2016.

[34] ANNAMALAI. S. A multivariate analysis and investigation on break even and productivity measures using artificial intelligence: A post research work in textile process industries. *Materials Today: Proceedings*. 2020.

[35] TANCO. M, CAT. L, GARAT. S. A break-even analysis for battery electric trucks in Latin America. *Journal of Cleaner Production, 228*, 1354-1367. 2019.

[36] SIMPSON. J .R, M12ISHRA .S, TALEBIAN .A, GOLIAS. M .M. An estimation of the future adoption rate of autonomous trucks by freight organizations. Research in Transportation Economics, 76, 100737. 2019.

[37] ISMAIL. Z, ABU. N. New car demand modeling and forecasting using bass diffusion model. American Journal of Applied Sciences, 10(6), 536. 2013.

[38] Lithuania in Europe. Statistics Lithuania. 2018.

[39] Statistical Yearbook of Lithuania. Edition -73. 2018.

[40] MCMANUS .W. Market models for predicting PHEV adoption and diffusion. University of Michigan, Ann Arbor, Transportation Research Institute. 2009.

[41] KOLAR .E, LINDSTRÖM .L. Future Business Model for OEMs in the Automotive Industry Business Model Adaptation Based on the Role an OEM Takes in a Future Business Network (Master's thesis). 2018.

[42] WELLS .P. Sustainable business models and the automotive industry: A commentary. IMB Management Review, 25(4), 228-239. 2013.

[43] FRITSCHY .C, SPINLER .S. The impact of autonomous trucks on business models in the automotive and logistics industry–a Delphi-based scenario study. Technological Forecasting and Social Change, 148, 119736. 2019.

[44] MONIOS .J, BERGQVIST. R. The transport geography of electric and autonomous vehicles in road freight networks. Journal of Transport Geography, 80, 102500. 2019.

[45] KALTENHÄUSER .B, WERDICH .K, DANDL .F, BOGENBERGER .K. Market development of autonomous driving in Germany. Transportation Research Part A: Policy and Practice, 132, 882-910. 2020.

[46] RASLAVIČIUS .L, AZZOPARDI .B, KERŠYS .A, STAREVIČIUS .M, BAZARAS .Ž, MAKARAS .R. Electric vehicles challenges and opportunities: Lithuanian review. Renewable and Sustainable Energy Reviews, 42, 786-800. 2015.

Appendix

The calculation of damping coefficient and critical damping coefficient is explained below,

Calculation of (-k/m) for MATLAB Input

Stiffness of Spring (k) = 3.567 N/mm, Mass (m) = 15 kg

(Top plate +Counterweight=Mass)

k/m = 0.2378

Where, ($-k/m$) = -0.2378

Calculation of (-c/m) for MATLAB Input

5 V Sample 1

ω_1 = 2Hz, ω_2 = 6Hz, ω_n= 4Hz

R.M.S Value = (Maximum Value)/√2 = 14.19Hz

$\xi = (\omega_1-\omega_2) / (2*\omega_n) = (2-6)/(2* 4) = -1$

m = 15 kg

$C_c = 2* m * \omega_n = 2 * 15 * 4 = 120$

$C = \xi * C_c = 1*120 = 120$

$C/m = 120/15 = 8$

Where, ($-C/m$) = -8

5 V Sample 2

ω_1 = 2Hz, ω_2 = 6.4Hz, ω_n= 4Hz

R.M.S Value = (Maximum Value)/√2 = 2.851Hz

$\xi = (\omega_1-\omega_2) / (2*\omega_n) = (2-6.4)/(2* 4) = -0.55$

m = 15 kg

$C_c = 2* m * \omega_n = 2 * 15 * 4 = 120$

$C = \xi * C_c = 0.55*120 = 66$

C/m = 66/15 = 4.4

Where, (-C/m) = -4.4

5 V Sample 3

ω_1 = 2Hz, ω_2 = 5.6Hz, ω_n= 4Hz

R.M.S Value = (Maximum Value)/√2 = 3.61Hz

$\xi = (\omega_1-\omega_2) / (2*\omega_n) = (2-5.6)/(2* 4) = -0.45$

m = 15 kg

$C_c = 2* m * \omega_n = 2 * 15 * 4 = 120$

$C = \xi * C_c = 0.45*120 = 54$

$C/m = 54/15 = 3.6$

Where, (-C/m) = -3.6

10 V Sample 1

ω_1 = 1.6Hz, ω_2 = 7.8Hz, ω_n= 4Hz

R.M.S Value = (Maximum Value)/√2 = 2.312Hz

$\xi = (\omega_1-\omega_2) / (2*\omega_n) = (1.6-7.8)/(2* 4) = -0.775$

m = 15 kg

$C_c = 2* m * \omega_n = 2 * 15 * 4 = 120$

$C = \xi * C_c = 0.775*120 = 93$

$C/m = 93/15 = 6.2$

Where, (-C/m) = -6.2

10 V Sample 2

ω_1 = 2.6Hz, ω_2 = 5.6Hz, ω_n= 4Hz

R.M.S Value = (Maximum Value)/√2 = 4.078Hz

$\xi = (\omega_1-\omega_2) / (2*\omega_n) = (2.6-5.6)/(2* 4) = -0.375$

m = 15 kg

C_c = 2* m * ω_n= 2 * 15 * 4 = 120

$C = \xi * C_c$ = 0.375*120 = 45

C/m = 45/15 = 3

Where, (-C/m) = -3

10 V Sample 3

ω_1 = 1.8Hz, ω_2 = 7.4Hz, ω_n= 4Hz

R.M.S Value = (Maximum Value)/√2 = 3.457Hz

$\xi = (\omega_1-\omega_2) / (2*\omega_n)$ = (1.8-7.4)/(2* 4) = -0.7

m = 15 kg

C_c = 2* m * ω_n= 2 * 15 * 4 = 120

$C = \xi * C_c$ = 0.7*120 = 84

C/m = 84/15 = 5.6

Where, (-C/m) = -5.6

15 V Sample 1

ω_1 = 2Hz, ω_2 = 5.8Hz, ω_n= 4Hz

R.M.S Value = (Maximum Value)/√2 = 14.509Hz

$\xi = (\omega_1-\omega_2) / (2*\omega_n)$ = (2-5.8)/(2* 4) = -0.475

m = 15 kg

C_c = 2* m * ω_n= 2 * 15 * 4 = 120

$C = \xi * C_c$ = 0.475*120 = 57

C/m = 57/15 = 4.4

Where, (-C/m) = -4.4

15 V Sample 2

ω_1 = 2.6Hz, ω_2 = 6Hz, ω_n= 4Hz

R.M.S Value = (Maximum Value)/√2 = 6.074Hz

$\xi = (\omega_1-\omega_2) / (2*\omega_n) = (2.6-6)/(2* 4) = -0.425$

m = 15 kg

$C_c = 2* m * \omega_n = 2 * 15 * 4 = 120$

$C = \xi * C_c = 0.425*120 = 51$

$C/m = 51/15 = 3.4$

Where, $(-C/m) = -3.4$

15 V Sample 3

ω_1 = 2.6Hz, ω_2 = 6Hz, ω_n= 4Hz

R.M.S Value = (Maximum Value)/√2 = 3.321Hz

$\xi = (\omega_1-\omega_2) / (2*\omega_n) = (2.6-6)/(2* 4) = -0.425$

m = 15 kg

$C_c = 2* m * \omega_n = 2 * 15 * 4 = 120$

$C = \xi * C_c = 0.425*120 = 51$

$C/m = 66/15 = 3.4$

Where, $(-C/m) = -3.4$

20 V Sample 1

ω_1 = 2Hz, ω_2 = 6Hz, ω_n= 4Hz

R.M.S Value = (Maximum Value)/√2 = 13.852Hz

$\xi = (\omega_1-\omega_2) / (2*\omega_n) = (2-6)/(2* 4) = -0.5$

m = 15 kg

$C_c = 2* m * \omega_n = 2 * 15 * 4 = 120$

$C = \xi * C_c = 0.5*120 = 60$

$C/m = 66/15 = 4$

Where, (-C/m) = -4

20 V Sample 2

ω_1 = 2.2Hz, ω_2 = 5.8Hz, ω_n= 4Hz

R.M.S Value = (Maximum Value)/√2 = 6.528Hz

ξ = (ω_1-ω_2) / (2*ω_n) = (2.2-5.8)/(2* 4) = -0.45

m = 15 kg

C_c = 2* m * ω_n= 2 * 15 * 4 = 120

C = ξ * C_c = 0.425*120 = 54

C/m = 66/15 = 3.6

Where, (-C/m) = -3.6

20 V Sample 3

ω_1 = 2.2Hz, ω_2 = 6.4Hz, ω_n= 4Hz

R.M.S Value = (Maximum Value)/√2 = 4.079Hz

ξ = (ω_1-ω_2) / (2*ω_n) = (2-6.4)/(2* 4) = -0.55

m = 15 kg

C_c = 2* m * ω_n= 2 * 15 * 4 = 120

C = ξ * C_c = 0.475*120 = 57

C/m = 66/15 = 3.8

Where, (-C/m) = -3.8